Molecular Cell



Article

Unprocessed genomic uracil as a source of DNA replication stress in cancer cells

Sneha Saxena,¹ Christopher S. Nabel,¹,²,² Turner W. Seay,³,² Parasvi S. Patel,¹,² Ajinkya S. Kawale,¹ Caroline R. Crosby,² Helene Tigro,³ Eugene Oh,¹ Matthew G. Vander Heiden,²,⁴ Aaron N. Hata,¹,⁵ Zucai Suo,³ and Lee Zou¹,6,7,9,*

¹Mass General Cancer Center, Harvard Medical School, Charlestown, MA, USA

*Correspondence: lee.zou@duke.edu https://doi.org/10.1016/j.molcel.2024.04.004

SUMMARY

Alterations of bases in DNA constitute a major source of genomic instability. It is believed that base alterations trigger base excision repair (BER), generating DNA repair intermediates interfering with DNA replication. Here, we show that genomic uracil, a common type of base alteration, induces DNA replication stress (RS) without being processed by BER. In the absence of uracil DNA glycosylase (UNG), genomic uracil accumulates to high levels, DNA replication forks slow down, and PrimPol-mediated repriming is enhanced, generating single-stranded gaps in nascent DNA. ATR inhibition in UNG-deficient cells blocks the repair of uracil-induced gaps, increasing replication fork collapse and cell death. Notably, a subset of cancer cells upregulates UNG2 to suppress genomic uracil and limit RS, and these cancer cells are hypersensitive to co-treatment with ATR inhibitors and drugs increasing genomic uracil. These results reveal unprocessed genomic uracil as an unexpected source of RS and a targetable vulnerability of cancer cells.

INTRODUCTION

Complete and accurate DNA replication is essential for the maintenance of genomic integrity. However, the progression of DNA replication forks is often impeded by various types of barriers or interferences, resulting in DNA replication stress (RS).^{1,2} Increased RS is commonly observed in cancer cells, which contributes to the genomic instability in cancer cells but also presents a vulnerability of cancer cells that can be targeted therapeutically.^{3–6} Understanding the sources of RS in cancer cells is critical for delineating the process of tumorigenesis and developing strategies to exploit RS in cancer therapy.

The common impediments or interferences to DNA replication forks can be divided into at least three classes. The first class comprises various types of physical barriers to replication forks, including bulky DNA adducts, DNA crosslinks, protein-DNA crosslinks, R-loops, transcription-replication conflicts, and others. ⁷⁻⁹ The second class includes various causes of insufficient deoxyribonucleotide triphosphate (dNTP) supply, which limits the activity of DNA polymerases. ¹⁰ The third class includes base alternations in DNA, such as those caused by guanine

oxidation, cytosine deamination, ten-eleven translocation (TET) enzymes-mediated cytosine demethylation, and misincorporation of uracil into DNA. 11 These base alterations trigger base excision repair (BER), generating abasic (AP) sites and DNA single-strand breaks (SSBs) as repair intermediates 12 (Figure 1A). AP sites and SSBs, if not removed timely and properly, can interfere with replication forks and generate DNA double-stranded breaks (DSBs). 13,14 Although base alterations are implicated in the generation of RS, it is still unclear whether this type of RS is always dependent on BER.

In cancer cells, the levels of base alterations in DNA are often elevated by the increase of reactive oxygen species (ROS), ¹⁵ aberrant expression of activation-induced cytidine deaminase (AID) and apolipoprotein B mRNA editing catalytic polypeptide-like (APOBEC) cytidine deaminases, ^{16,17} and changes in dUTP and dTTP biogenesis. ¹⁸ Thus, increased base alterations in DNA constitute an important source of RS in cancer cells and potentially provide an opportunity for targeted therapy. The ataxia telangiectasia-mutated and Rad3-related (ATR) kinase is a master regulator of the cellular response to RS, and it is critical for cancer cells to cope with RS and genomic instability. ^{4,19,20}

²Koch Institute for Integrative Cancer Research, Massachusetts Institute of Technology, Cambridge, MA, USA

³Department of Biomedical Sciences, Florida State University, Tallahassee, FL, USA

⁴Department of Medical Oncology, Dana Farber Cancer Institute, Boston, MA, USA

⁵Department of Medicine, Massachusetts General Hospital, Harvard Medical School, Boston, MA, USA

⁶Department of Pathology, Massachusetts General Hospital, Harvard Medical School, Boston, MA, USA

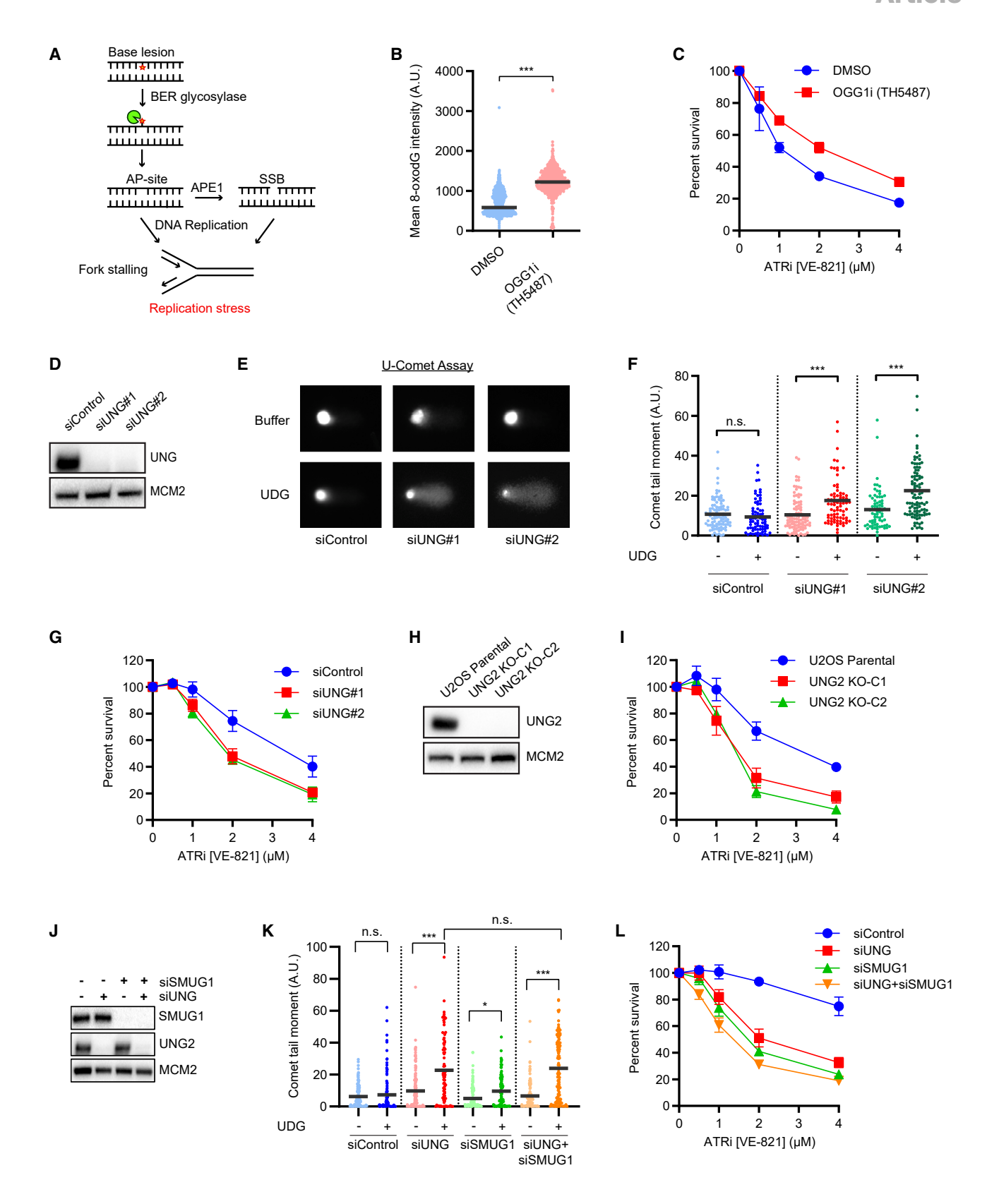
⁷Department of Pharmacology and Cancer Biology, Duke University School of Medicine, Durham, NC, USA

⁸These authors contributed equally

⁹Lead contact

CellPress

Molecular CellArticle



(legend on next page)



Recently, ATR inhibitors (ATRis) have been successfully used to eliminate cancer cells under specific oncogene-induced RS. ^{21,22} However, it remains unclear whether ATRi can effectively kill cancer cells harboring high levels of base alterations and whether BER intermediates are important for ATRi sensitivity. Furthermore, whether different types of base alterations generate RS and confer ATRi sensitivity through the same or distinct mechanisms remains unknown.

RESULTS

Processing of genomic uracil by UNG2 reduces ATRi sensitivity

To test whether base alterations induce RS and confer ATRi sensitivity through BER intermediates, we sought to ablate various DNA glycosylases, the enzymes that recognize different types of base alterations and initiate BER (Figure 1A). We first inhibited OGG1, the DNA glycosylase that recognizes and processes 8-oxidized guanine (oxoG), in U2OS cells with the OGG1 inhibitor (OGG1i) TH5487.²³ As expected, OGG1i increased the levels of 8-oxoG in cells (Figure 1B), confirming that the conversion of 8-oxoG to AP site by OGG1, the first step of BER, was inhibited. OGG1i reduced the sensitivity of cells to two distinct ATRis, VE-821 and AZD6738 (Figures 1C and S1A). Similar results were obtained with small interfering RNA (siRNA)-mediated knockdown of OGG1 (Figures S1B and S1C), supporting the idea that 8-oxoG confers ATRi sensitivity through BER.

Next, we tested whether the deoxyuracil (dU) in DNA also confers ATRi sensitivity through BER. Uracil in DNA is a common base alteration resulting from the misincorporation of dUTP during DNA replication or deamination of cytosine. The uracil glycosylases UNG1 and UNG2, which are encoded by two isoforms of the *UNG* gene, are the primary enzymes that recognize and process the uracil in DNA.²⁴ Whereas UNG1 localizes to mitochondria, UNG2 functions in the nucleus. We used two independent siRNAs, each targeting both isoforms of *UNG*, to deplete UNG in U2OS cells (Figures 1D and S1D). To confirm the effects of UNG loss, we used a modified comet assay (U-comet) to measure uracil levels in genomic DNA (Figure 1E). In this assay, cells were treated with recombinant uracil DNA glycosylase (UDG)

before being analyzed by the alkaline comet protocol, allowing detection of DNA breakage at sites of genomic uracil. As expected, UNG knockdown increased genomic uracil (Figures 1E, 1F, and S1E), which was associated with a concomitant reduction in AP sites (Figure S1F), showing that the uracil in DNA was not efficiently processed in the absence of UNG. Surprisingly, however, knockdown of UNG increased the ATRi sensitivity of cells (Figures 1G and S1G), suggesting that BER does not enhance ATRi sensitivity in this context. Expression of HAtagged UNG2 substantially reversed the increase of ATRi sensitivity in UNG knockdown cells (Figures S1H and S1I), confirming that the effect of UNG knockdown on ATRi sensitivity is largely, if not completely, attributed to UNG2 loss. To confirm the results from UNG knockdown cells and test whether UNG2 loss is responsible for increased ATRi sensitivity, we generated 2 independent UNG2 knockout (KO) cell lines using CRISPR-Cas9. Notably, western blot with the UNG antibody showed a complete loss of signal in UNG2 KO cells (Figure 1H), indicating that the detected band is specific to UNG2. Henceforth, we used this antibody as a UNG2 antibody. As expected, the levels of genomic uracil were higher in UNG2 KO lines than in the parental line (Figure S1J). Similar to UNG knockdown cells, the UNG2 KO cell lines were more sensitive to ATRi than parental U2OS cells (Figures 1I and S1K).

In addition to UNG, three other DNA glycosylases—SMUG1, MBD4, and TDG-have been implicated in the processing of genomic uracil in specific contexts.²⁵ SMUG1 excises 5-hydroxymethyl uracil (5-hmdU) and is a possible backup for UNG for removing uracil in specific sequence contexts. 14,26 MBD4 and TDG are primarily involved in removing the thymine generated by the deamination of 5-methylcytosine but also remove a variety of other base lesions, including U in G:U pairs.²⁷ To test whether these glycosylases compensate for the loss of UNG to confer ATRi sensitivity, we co-depleted these enzymes with UNG. Loss of SMUG1 alone slightly increased genomic uracil. but co-depletion of UNG and SMUG1 did not increase genomic uracil more than UNG loss alone (Figures 1J and 1K), showing that SMUG1 does not function as a backup for UNG loss in suppressing overall genomic uracil levels. Furthermore, knockdown of SMUG1 alone increased ATRi sensitivity, and co-depletion of UNG and SMUG1 modestly increased ATRi

Figure 1. UNG2-mediated processing of genomic uracil reduces ATRi sensitivity

(A) A schematic of RS induction by BER intermediates—AP sites and SSBs.

(B) Quantification of 8-oxoG immunofluorescence in cells treated with DMSO or 10 μ M TH5487 for 6 h (n > 900 cells per condition). One of two independent experiments is shown.

(C) U2OS cells were treated with DMSO or 10 μ M TH5487 and indicated concentrations of ATRi (VE-821) for 5–7 days. Cell viability was determined using CellTiter-Glo. Data are shown as mean \pm SD. (n = 2 independent experiments).

(D) Levels of UNG in U2OS cells transfected with the indicated siRNAs for 48 h. MCM2 serves as a loading control.

(E and F) Representative images for U-comet assay in U2OS cells transfected with indicated siRNAs. Dot plots represent comet tail moment in individual cells, and bars display the mean in cell populations (n > 70 cells per condition). ns, non-significant. *** $p \le 0.001$. One of three experiments is shown.

(G) Viability of U2OS cells transfected with indicated siRNAs and treated with indicated concentrations of ATRi (VE-821). Data are shown as mean ± SD. (n = 2 independent experiments).

(H) Levels of UNG2 in U2OS cells and two independent UNG2-/- knockout (KO) clones. MCM2 serves as a loading control.

(I) Viability of U2OS or UNG2 KO cells treated with indicated concentrations of ATRi (VE-821). Data are shown as mean ± SD. (n = 2 independent experiments).

(J) Levels of the indicated proteins in U2OS cells transfected with UNG#1 and SMUG1 siRNAs for 48 h. MCM2 serves as a loading control.

(K) U2OS cells transfected with UNG#1 and SMUG1 siRNAs were analyzed by U-comet assay (n > 80 cells per condition). One of two experiments is shown. (L) Viability of U2OS cells transfected with UNG#1 and SMUG1 siRNAs and treated with indicated concentrations of ATRi (VE-821). Data are shown as mean ± SD. (n = 3 independent experiments).



sensitivity more than single depletions of UNG and SMUG1 (Figure 1L), suggesting that the uracil derivatives suppressed by SMUG1, such as 5-hmdU, may also increase ATRi sensitivity. Unlike loss of UNG and SMUG1, depletion of MBD4 or TDG did not affect the overall levels of genomic uracil (Figures S1L-S1N). When combined with UNG knockdown, neither MBD4 nor TDG depletion increased genomic uracil levels further (Figures S1M and S1N). Furthermore, depletion of MBD4 or TDG in UNG knockdown cells did not reduce but increased ATRi sensitivity (Figures S10 and S1P), suggesting that these glycosylases do not compensate for UNG loss to confer ATRi sensitivity by generating BER intermediates. Finally, we used an in vitro biochemical assay to test whether the uracil glycosylase activity in cell extracts was compensated by other enzymes upon UNG loss. Depletion of UNG eliminated the detectable uracil glycosylase activity in cell extracts (Figure S1Q), showing that the loss of UNG activity is not compensated by any other enzymes. Together, these results strongly support the notion that the accumulation of genomic uracil increases ATRi sensitivity in the absence of BER.

Unprocessed genomic uracil impedes replication forks

To directly test whether genomic uracil affects the progression of replication forks, we used DNA fiber assay to analyze UNG knockdown cells. In cells treated with increasing concentrations of UNG siRNA, UNG was depleted, and replication fork speed was reduced in a manner dependent on siRNA concentrations (Figures 2A and S2A). The slowing of replication forks upon UNG loss was also observed using multiple UNG siRNAs (Figures 2B and S2B) and UNG2 KO cell lines (Figure S2C). Thus, UNG promotes replication fork progression in a dose-dependent manner.

Next, we tested whether altered dUTP/dTTP ratio and subsequent misincorporation of dUTP to genomic DNA interferes with replication forks. We used pemetrexed (PMX), a folate analog that inhibits the thymidylate synthase (TYMS), which converts dUMP to dTMP.28 Treatment of cells with PMX is expected to reduce dTTP, increase the dUTP/dTTP ratio, and enhance uracil misincorporation. Indeed, as revealed by the U-comet assay, the levels of genomic uracil were increased by PMX treatment (Figure S2D). Notably, PMX further increased genomic uracil in UNG knockdown cells (Figure S2D), suggesting that the PMX-induced genomic uracil is removed by BER. In addition, liquid chromatography-mass spectrometry (LC-MS) confirmed that after PMX treatment, UNG2 KO cells contained more genomic uracil than parental U2OS cells (Figure S2E). Treatment of cells with PMX reduced fork speed in a dose-dependent manner (Figure 2C). Importantly, the effect of PMX on fork speed was reversed by supplementing cells with a low concentration of thymidine (Figure S2F), which increases dTTP levels but does not inhibit DNA synthesis by reducing the dCTP pool,²⁹ confirming that PMX decreases fork speed by reducing dTTP and increasing uracil misincorporation. Treatment of UNG knockdown cells with PMX further reduced fork speed (Figure 2D), showing that PMX affects fork progression independently of UNG-mediated BER. Together, these experiments suggest that PMX-induced reduction in dTTP and increase in dUTP misincorporation induce RS even when genomic uracil is not processed by BER.

To confirm that PMX-induced dUTP misincorporation contributes to RS, we sought to increase dUTP without altering dTTP. dUTPase is an enzyme that hydrolyzes dUTP to dUMP, which in turn serves as a precursor for thymidylate synthesis.³⁰ Inhibition of dUTPase is expected to increase the cellular dUTP pool and dUTP misincorporation, with minimal effect on dTTP pool.³¹ Indeed, the dUTPase inhibitor TAS-114 increased genomic uracil as measured by the U-comet assay (Figure S2G) and led to a modest increase in genomic uracil in UNG2 KO cells compared with parental U2OS cells as shown by LC-MS (Figure S2E). Similar to PMX, TAS-114 further reduced fork speed in cells lacking UNG (Figure 2E). We further validated these observations by siRNA-mediated knockdown of dUTPase, which also led to increased genomic uracil (Figure S2H), fork slowing (Figure S2I), and further reduced fork speed in UNG knockdown cells (Figure 2F). Together, the experiments using UNG-depleted cells, PMX-treated cells, TAS-114-treated cells, and dUTPasedepleted cells strongly suggest that unprocessed genomic uracil interferes with replication forks and induces RS.

Finally, we tested the effects of uracil in template DNA on the progression of human DNA polymerase epsilon (Polε) in vitro. We designed a 23-nt primer and two pairs of 44-nt DNA templates containing either one or two consecutive dUs (1U and 2U) or dTs at the same positions (1T and 2T). A purified human Polε catalytic fragment lacking the exonuclease activity (hPolε exo⁻) was previously used to study the function of Polε on various DNA templates.³²⁻³⁵ Using purified hPole exo⁻ and dU- or dT-containing DNA templates, we tested the effects of dU on Polε-mediated primer extension. As expected, full-length extension products were formed on both DNA templates in a time-dependent manner (Figures S2J and S2K). Notably, a band of an intermediate product was transiently observed on the 1U but not the 1T template (Figure S2J). Furthermore, high levels of intermediate products were detected on the 2U but not the 2T template (Figure S2K), suggesting that consecutive dUs slow polymerase more effectively. Together, these biochemical results support the notion that unprocessed uracil in template DNA impedes DNA synthesis and is a source of RS.

Genomic uracil induces PrimPol-generated ssDNA gaps

Stalling of DNA polymerase by barriers can lead to uncoupling of polymerase and the replicative helicase, resulting in the accumulation of RPA-coated single-stranded DNA (ssDNA) adjacent to stalled polymerase.³⁶ To test whether genomic uracil induces RPA accumulation next to Polε at stalled forks, we performed proximity ligase assay (PLA) with antibodies to the catalytic subunit of Pole and the RPA32 subunit of RPA. PLA foci were readily detected in hydroxyurea (HU)-treated cells when both Polε and RPA32 antibodies were applied, but not when either antibody was used individually (Figure S3A), validating this assay for the detection of RPA accumulation at stalled forks. Importantly, either PMX or TAS-114 treatment significantly increased PLA foci in both control cells and UNG knockdown cells (Figures 3A, 3B, and S3B), suggesting that genomic uracil induces RPA-ssDNA accumulation at stalled forks independently of UNG-mediated BER. Of note, accumulation of RPA-coated ssDNA at stalled replication forks triggers ATR activation.²⁰ Indeed, in UNG-depleted cells, both PMX and TAS-114



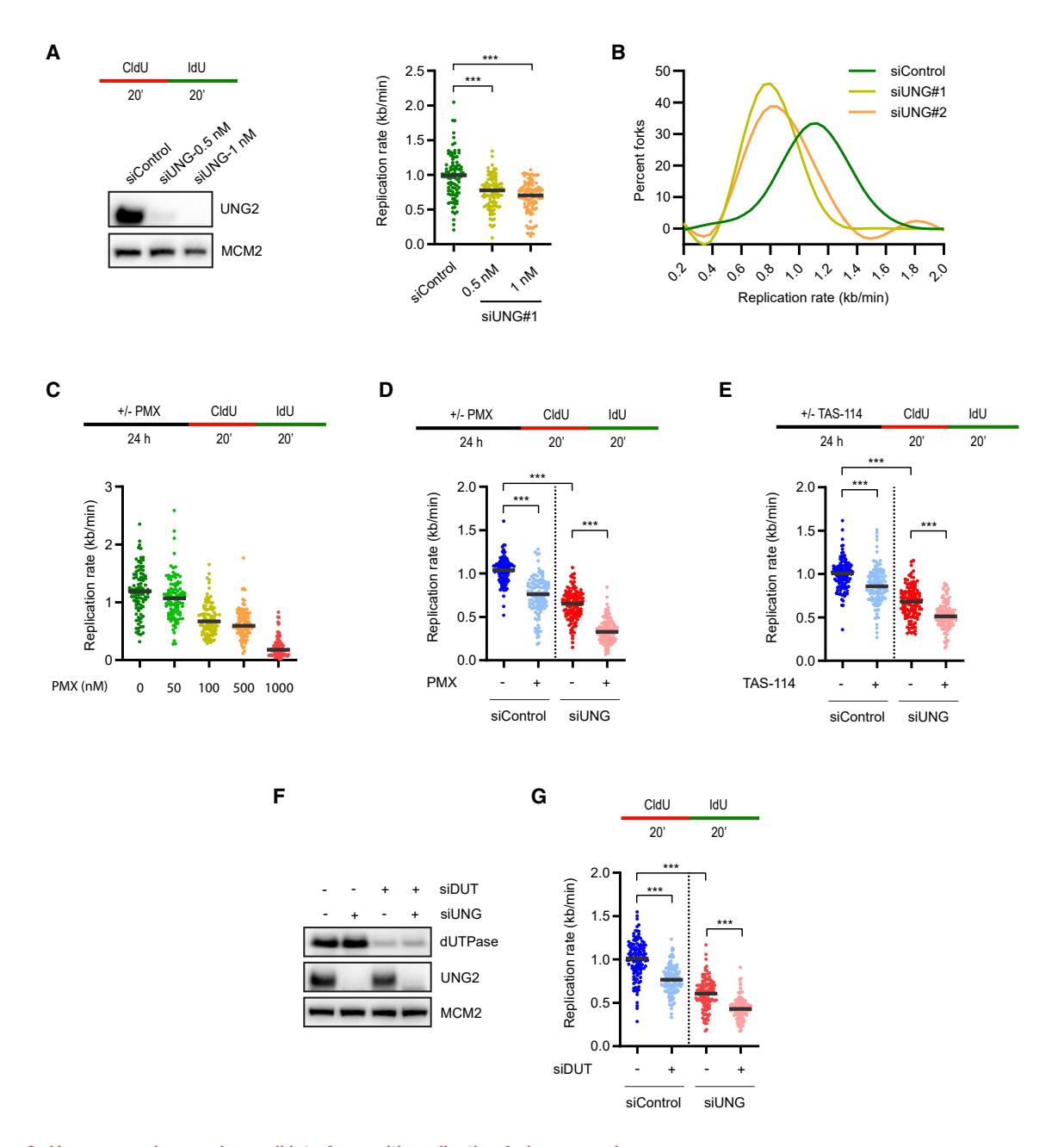


Figure 2. Unprocessed genomic uracil interferes with replication fork progression

(A) U2OS cells were transfected with indicated concentrations of UNG siRNA#1 for 48 h. Levels of UNG2 were analyzed by western blot, and the replication rate was analyzed by DNA fiber assay (n = 100 fibers per condition). MCM2 serves as a loading control. One of three independent experiments is shown. **** $p \le 0.001$. (B) The distribution of replication rate in U2OS cells treated with indicated siRNAs (n = 125 fibers per condition). One of two experiments is shown.

(C) Replication rate in U2OS cells treated with indicated concentrations of pemetrexed (PMX) for 24 h (n = 125 fibers per condition). One of two experiments is shown.

(D and E) Replication rate in U2OS cells transfected with control or UNG#1 siRNA for 48 h and treated with 200 nM PMX (D) or 10 μ M TAS-114 (E) for 24 h (n = 125 fibers per condition). One of two experiments is shown.

(F and G) U2OS cells were transfected with dUTPase (DUT) and UNG#1 siRNAs for 48 h. Levels of dUTPase and UNG2 were analyzed by western blot (F). MCM2 serves as a loading control. Replication rate was analyzed by DNA fiber assay (n = 125 fibers per condition) (G). One of two experiments is shown.

increased the phosphorylation of ATR substrates Chk1 (pS317) and RPA32 (pS33) (Figures S3C and S3D). Thus, unprocessed genomic uracil not only slows Polε but also activates the RS response through RPA-ssDNA.

DNA polymerase stalling and RPA-ssDNA accumulation at stalled forks also trigger PrimPol-mediated repriming, which enables resumption of DNA synthesis ahead of stalled polymerases but leaves ssDNA gaps in nascent DNA. 37–39 In cells treated



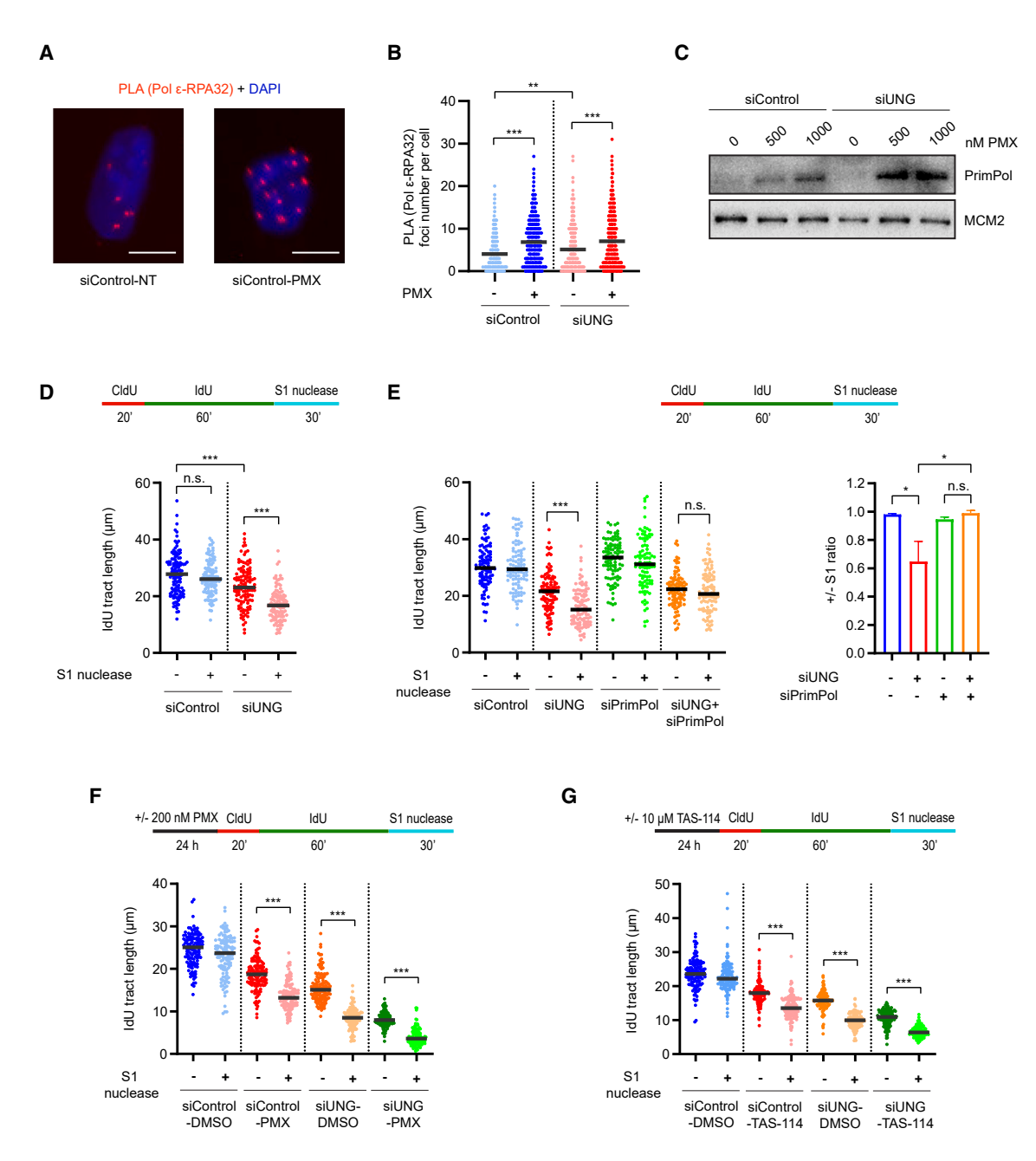


Figure 3. Genomic uracil induces PrimPol-dependent ssDNA gaps in nascent DNA

(A and B) U2OS cells transfected with control or UNG#1 siRNA and treated with 100 nM PMX for 24 h were analyzed by PLA using anti-Pol ε catalytic subunit and anti-RPA32 antibodies. Representative images of PLA foci are shown (A), and PLA foci are quantified in individual cells (B) (n > 400 cells per condition). Scale bars, 10 μ m. ** $p \le 0.01$. *** $p \le 0.001$. One of three independent experiments is shown.

(C) U2OS cells were transfected with control or UNG#1 siRNA and treated with indicated concentrations of PMX for 24 h. Chromatin fractions were prepared and blotted for PrimPol. MCM2 serves as a loading control.

(D) U2OS cells were transfected with control or UNG#1 siRNA for 48 h and analyzed by DNA fiber assay. DNA fibers were treated with S1 nuclease (20 U/mL) for 30 min at 37° C, and the length of IdU tracts (n = 125 fibers per condition) was measured. One of two experiments is shown.

(E) U2OS cells were transfected with UNG#1 and PrimPol siRNA for 48 h and analyzed as in (D) (n = 125 fibers per condition). One of two experiments is shown. Right, ratio of IdU tracts from S1-treated to -untreated fibers. Data are displayed as mean \pm SD. from two experiments. * $p \leq 0.05$.

(F) U2OS cells transfected with control or UNG#1 siRNA were treated with 200 nM PMX for 24 h and analyzed as in (D) (n = 125 fibers per condition). One of three experiments is shown.

(G) U2OS cells transfected with control or UNG#1 siRNA were treated with 10 μ M TAS-114 for 24 h and analyzed as in (D) (n = 125 fibers per condition). One of two experiments is shown.



with increasing concentrations of PMX, PrimPol was recruited onto chromatin in a PMX dose-dependent manner (Figure S3E). Furthermore, PMX further increased the levels of chromatin-bound PrimPol in UNG knockdown cells (Figure 3C). Similar results were obtained with TAS-114 (Figure S3F), suggesting that genomic uracil promotes the recruitment of PrimPol to stalled forks independently of UNG-mediated BER.

To directly test whether genomic uracil induces PrimPol-mediated ssDNA gaps, we treated DNA fibers with the S1 nuclease, which specifically cleaves ssDNA.40 If ssDNA gaps are present in nascent DNA, replication tracts should be shortened by S1. Knockdown of UNG significantly increased the shortening of replication tracts by S1 (Figures 3D and S3G), and similar observations were made in UNG2 KO cell lines (Figures S3I and S3J), showing that UNG loss increases ssDNA gaps. Notably, the increase of S1 cleavage of replication tracts in UNG knockdown and UNG2 KO cells was not observed when PrimPol was codepleted (Figures 3E and S3H-S3J), showing that ssDNA gaps were formed in a PrimPol-dependent manner. We noted that loss of PrimPol did not significantly alter fork speed in control, UNG knockdown, and UNG2 KO cells (Figures 3E and S3J), suggesting the presence of a backup pathway. Inhibition of translesion DNA synthesis (TLS) in cells lacking UNG and PrimPol further reduced fork speed (Figure S3K), suggesting that TLS acts as an alternative mechanism to sustain fork progression in the presence of uracil and the absence of PrimPol.

Treatment with PMX or TAS-114, as well as knockdown of dUTPase, increased the shortening of replication tracts by S1 (Figures 3F, 3G, S3L, and S3M), supporting the idea that genomic uracil induces ssDNA gaps. Knockdown of PrimPol prevented the shortening of replication tracts by S1 in PMXtreated cells (Figure S3N), showing that the ssDNA gaps formed in this context were also PrimPol-dependent. In UNG knockdown cells, replication tracts were further shortened by PMX treatment or dUTPase inhibition/depletion (Figures 3F, 3G, S3L, and S3M), reflecting a further increase of genomic uracil. Notably, these short tracts were still efficiently cleaved by S1 (Figures 3F, 3G, S3L, and S3M), suggesting that ssDNA gaps were formed independently of UNG-mediated BER. Supplementing UNG knockdown cells with thymidine reduced the cleavage of replication tracts by S1 (Figure S3O, lanes 1-4). In the presence of PMX, thymidine partially rescued fork speed in UNG knockdown cells and also reduced S1 cleavage (Figure S3O, lanes 5-8). Thus, unprocessed genomic uracil, which is increased by UNG loss and PMX/TAS-114-induced uracil misincorporation, induces PrimPol-generated ssDNA gaps.

Exogenous dUTP induces RS

To test the effects of dUTP misincorporation on replication forks more directly, we sought to directly increase dUTP levels in cells. Because dNTPs do not permeate cell membranes efficiently, we tested whether a recently developed synthetic nucleoside triphosphate transporter (henceforth termed Bio-Tracker, BT) can transport dUTP into cells. He first tested BT with Cy3-labeled dUTP and validated the import of Cy3-dUTP into U2OS cells (Figure 4A). Using DNA fiber assay, we confirmed that BT-imported Cy3-dUTP was incorporated into genomic DNA (Figure 4A). As expected, our U-comet assay showed a signifi-

cant increase of genomic uracil in cells treated with BT and Cy3-dUTP (Figure 4B). These experiments established a strategy to directly increase the dUTP pool in cells and dUTP misincorporation into the genome.

Next, we sought to characterize the cellular response to genomic uracil using this system. Import of Cy3-dUTP reduced fork speed in a dose-dependent manner (Figure 4C). Importantly, when increasing concentrations of dTTP were co-imported with Cy3-dUTP, the Cy3-dUTP-induced fork slowing was alleviated by dTTP in a dose-dependent manner (Figure 4D). Similar observations were made using unlabeled dUTP and dTTP (Figure 4E), ruling out unexpected effects of Cy3. Furthermore, dTTP also suppressed the increase of genomic uracil induced by Cy3-dUTP in a concentration-dependent manner (Figure S4A). These results strongly suggest that the dUTP/dTTP ratio is a key determinant of genomic uracil levels.

Using DNA fiber assay and the S1 nuclease, we confirmed that both Cy3-dUTP and unlabeled dUTP, but not dTTP, induced ssDNA gaps in nascent DNA (Figures 4F and S4B). Furthermore, the induction of ssDNA gaps by Cy3-dUTP was dependent on PrimPol (Figures 4F and S4C). Notably, even in UNG knockdown cells, Cy3-dUTP further shortened replication tracts, and the short tracts were still sensitive to S1 cleavage (Figure 4G), suggesting that unprocessed genomic uracil impedes replication forks and induces ssDNA gaps. At a low concentration that did not change the ATRi sensitivity of cells treated with control siRNA, Cy3-dUTP increased the ATRi sensitivity of UNG knockdown cells (Figure S4D), supporting the notion that dUTP misincorporation increases unprocessed genomic uracil and associated RS.

ATR is required for the repair of uracil-induced ssDNA gaps

Next, we investigated how genomic uracil enhances ATRi sensitivity. PrimPol-generated ssDNA gaps, if not repaired properly, can persist into the next cell cycle, collide with replication forks, and give rise to DSBs. 42-44 To test whether ATR is involved in the repair of uracil-induced ssDNA gaps, we pulse-labeled nascent DNA in UNG knockdown cells and then let cells progress through the cell cycle in the presence or absence of ATRi (Figure 5A). If ssDNA gaps are formed during DNA labeling and subsequently repaired, ssDNA gaps should be gradually removed from labeled DNA over time. Using the S1 nuclease, we confirmed the increase of ssDNA gaps in UNG knockdown cells right after nascent DNA labeling (Figure 5A, lanes 1-4). In the absence of ATRi, ssDNA gaps gradually disappeared from labeled DNA after 8 and 24 h (Figure 5A, lanes 5-6), showing repair of the gaps. In the presence of ATRi, however, the removal of ssDNA gaps was significantly compromised (Figure 5A, lanes 7-8). Recent studies have implicated RAD51-mediated template switch (TS) and TLS in the repair of PrimPol-mediated ssDNA gaps. 43,44 In cells lacking UNG, inhibition of either RAD51 or TLS delayed gap removal (Figure S5A, lanes 7-8; Figure S5B, lanes 7-8), suggesting that both TS and TLS contribute to the repair of uracil-induced gaps. Together, these results suggest that ATR, RAD51, and TLS function in concert to repair ssDNA gaps, allowing cells to tolerate uracil-induced RS.

If ATRi prevents the repair of uracil-induced ssDNA gaps, these gaps may persist into the next cell cycle. To test this



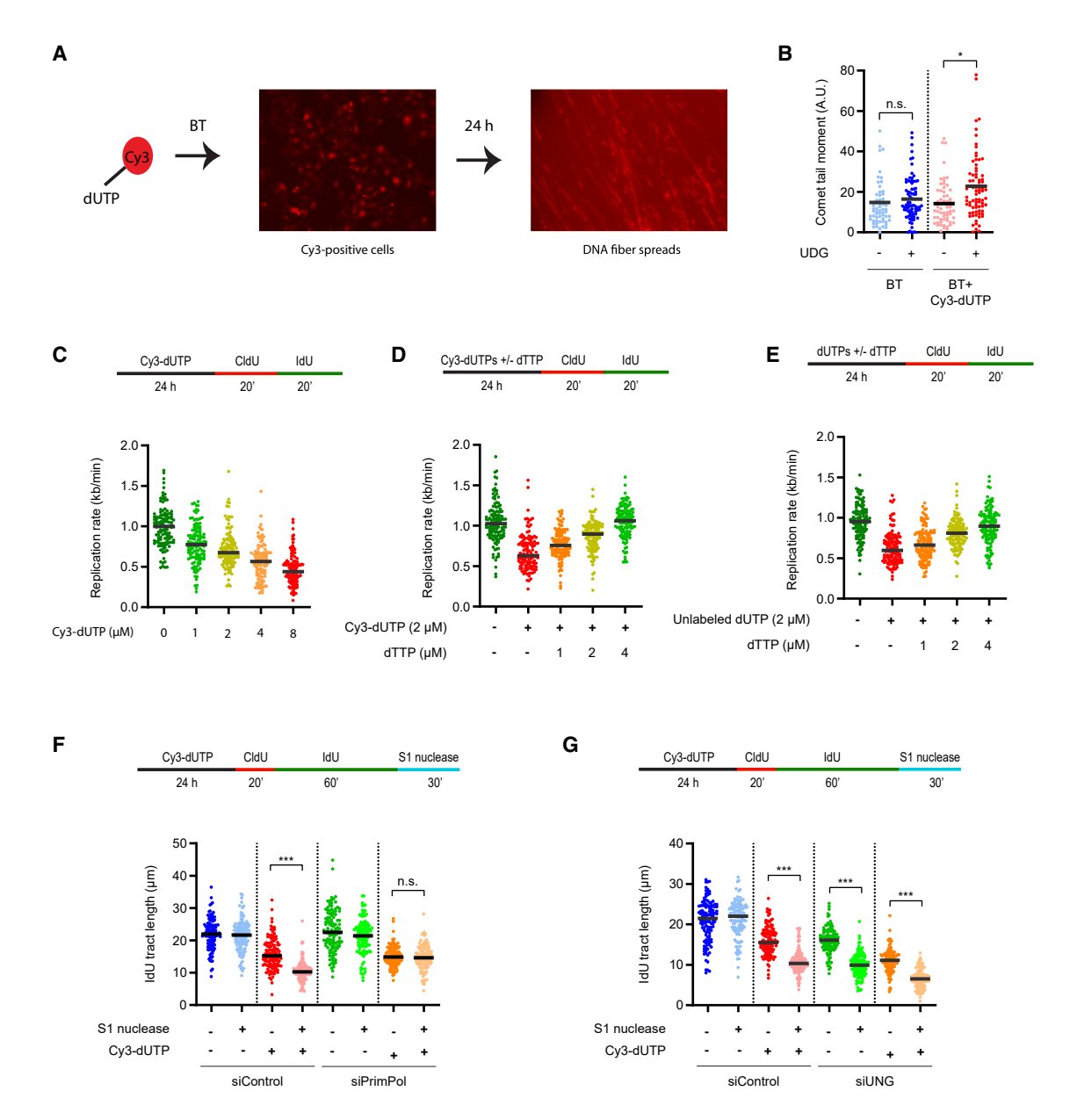
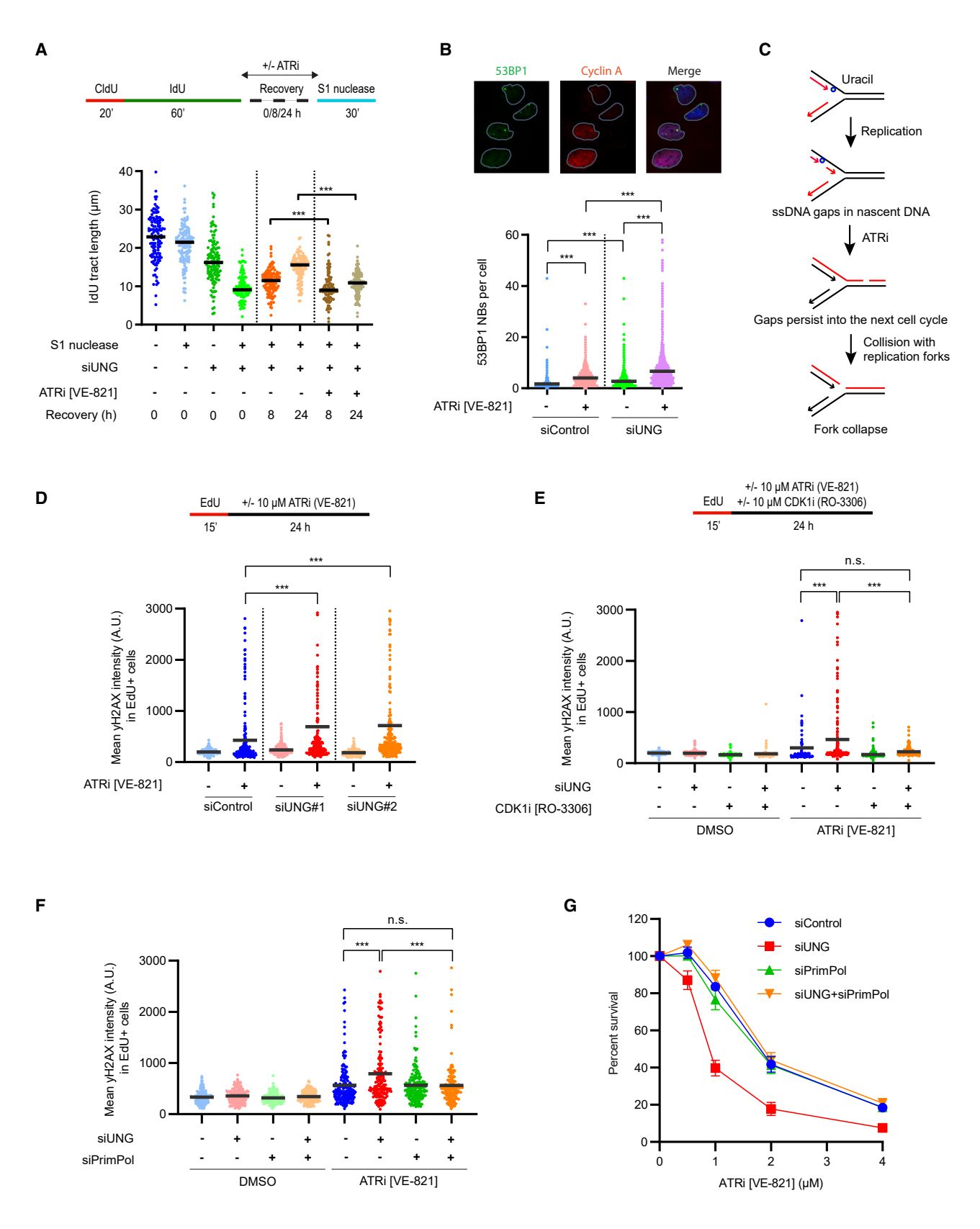


Figure 4. Exogenous dUTP supplementation induces replication stress

(A) A schematic of import of Cy3-dUTP into live cells by Bio-Tracker (BT). U2OS cells were treated with 2 μ M BT and 2 μ M Cy3-dUTP for 24 h in Leibovitz's L-15 medium and analyzed by fluorescence. After 24 h, cells were analyzed by DNA fiber to visualize the incorporation of Cy3-dUTPs into genomic DNA.

- (B) U2OS cells were treated with 2 μ M BT and 2 μ M Cy3-dUTP for 24 h and analyzed by U-comet assay (n > 50 cells per condition). One of two experiments is shown.
- (C) Replication rate in U2OS cells treated with 2 μ M BT and indicated concentrations of Cy3-dUTP for 24 h (n = 125 fibers per condition). One of two experiments is shown.
- (D) Replication rate in U2OS cells treated with 2 μ M BT, 2 μ M Cy3-dUTP, and indicated concentrations of dTTP for 24 h (n = 125 fibers per condition). One of two experiments is shown.
- (E) Replication rate in U2OS cells treated with 2 μ M BT, 2 μ M unlabeled dUTP, and indicated concentrations of dTTP for 24 h (n = 125 fibers per condition). One of two experiments is shown.
- (F) U2OS cells transfected with control or PrimPol siRNA were treated with 2 μ M BT and 2 μ M Cy3-dUTP for 24 h. DNA fibers were treated with S1 nuclease, and the length of IdU tracts (n = 125 fibers per condition) was measured. One of two experiments is shown.
- (G) U2OS cells were transfected with control or UNG#1 siRNA, treated with 2 μ M BT and 2 μ M Cy3-dUTP for 24 h, and analyzed as in (F) (n = 125 fibers per condition). One of two experiments is shown.





(legend on next page)



possibility, we analyzed whether the 53BP1 nuclear bodies (NBs) in G1 phase are affected by ATRi in UNG knockdown cells. G1 53BP1 NBs are induced by RS and associated with under-replicated DNA. 45,46 In the absence of ATRi, 53BP1 NB levels in cyclin A-negative G1 cells were higher in the UNG knockdown cell population than in the control cell population (Figure 5B), consistent with the induction of RS by UNG loss. In the presence of ATRi, 53BP1 NBs were further increased in UNG knockdown cells (Figure 5B), suggesting that more under-replicated DNA persisted into the next G1. These results raised the possibility that uracil-induced ssDNA gaps can persist into the next S phase in the presence of ATRi, leading to replication fork collapse⁴² (Figure 5C). To test this idea, we pulse-labeled S phase cells with EdU and then treated them with ATRi for 24 h to analyze the effects of ATR in these cells in the second cell cycle. ATRiinduced γH2AX was significantly higher in EdU+ UNG knockdown cells than in EdU+ control cells (Figure 5D), suggesting that genomic uracil promotes ATRi-induced DSB formation. By contrast, knockdown of OGG1 reduced ATRi-induced γH2AX (Figure S5C), consistent with the notion that 8-oxoG-induced BER intermediates drive RS. Blocking the cell cycle at the G2/ M transition with the CDK1 inhibitor R0-3306 drastically reduced ATRi-induced γH2AX in UNG knockdown cells (Figure 5E), showing that the entry to the next cell cycle is required for ATRi-induced DSB formation. Importantly, knockdown of PrimPol reversed the induction of YH2AX in the UNG-depleted cells (Figure 5F), confirming that the DSBs arose from PrimPolgenerated ssDNA gaps. Remarkably, co-depletion of PrimPol in UNG knockdown cells completely reversed the increase of ATRi sensitivity (Figures 5G and S5D), lending further support to the notion that the ATRi sensitivity of UNG knockdown cells is attributed to PrimPol-generated ssDNA gaps. Together, these results suggest that ATRi induces gap-derived DSBs in UNGdepleted cells in a trans-cell-cycle manner.

To understand how replication forks collapse in ATRi-treated UNG knockdown cells, we asked whether nucleases are involved. The DNA structure-specific nucleases MUS81 and MRE11 have been implicated in the collapse of replication forks. 47,48 Knockdown of MUS81 and inhibition of MRE11 with Mirin both significantly suppressed ATRi-induced $\gamma H2AX$ in UNG knockdown cells in the second S phase (Figures S5E–S5G), suggesting that both of these nucleases are involved in the accumulation of ATRi-induced DSBs in UNG-depleted cells. It is possible that when the repair of uracil-induced gaps is

compromised by ATRi, these gaps or the forks approaching them need to be processed by MRE11 and MUS81 to form DSBs efficiently.

High UNG expression in cancer cells is associated with uracil-induced RS

The role of UNG in limiting genomic uracil and RS raises the possibility that UNG may be upregulated in a subset of cancers to allow cancer cells to cope with uracil-induced RS. Notably, UNG2 is commonly expressed at higher levels in lung cancer cell lines compared with non-malignant lung epithelial cells.⁴⁹ To test whether cancer cells expressing high levels of UNG2 depend on it to suppress genomic uracil and RS, we analyzed UNG2 protein levels in a panel of lung cancer cell lines (Figure 6A). Among the cell lines, only H1299 expresses UNG2 at high levels. No correlation between UNG2 protein levels and ATRi sensitivity was observed in these cell lines (Figure S6A). However, when UNG was knocked down in these cell lines, H1299, but not the other cell lines, became significantly more sensitive to ATRi (Figures 6B and S6B). These results suggest that H1299, which expresses UNG2 at the highest level in this cell line panel, is the most dependent on UNG2 to suppress RS. Similar to the cancer cell lines expressing low levels of UNG2, RPE-1, a non-transformed cell line, expressed UNG2 at a low level and exhibited only a modest increase in ATRi sensitivity upon UNG knockdown (Figure S6C).

To directly compare the levels of genomic uracil in the lung cancer cell lines, we analyzed H1299 and H1838, which express low levels of UNG2 (Figure 6A), with U-comet assay. Upon UNG knockdown, a drastic increase of genomic uracil was detected in H1299 but not in H1838 (Figure 6C). These results demonstrate that H1299 is more dependent on UNG2 than H1838 to suppress genomic uracil, providing an example of the UNG2 dependency of cancer cells.

To characterize the RS in cancer cells expressing high or low levels of UNG2, we analyzed H1299 and H1838 with DNA fiber assay. Knockdown of UNG drastically reduced replication fork speed in H1299 cells and increased ssDNA gaps in a PrimPoldependent manner (Figures 6D, S6D, and S6E). By contrast, UNG loss did not affect fork speed and only slightly increased ssDNA gaps in H1838 cells (Figures 6D and S6D). Furthermore, in H1299, PrimPol knockdown significantly reversed the increase of ATRi sensitivity induced by UNG loss (Figure 6E). In H1838, PrimPol knockdown modestly increased ATRi resistance and

Figure 5. ATRi prevents repair of uracil-induced ssDNA gaps and increases DNA damage

(A) U2OS cells were transfected with control or UNG#1 siRNA, sequentially labeled with CldU and IdU, and cultured in the presence or absence of 10 μM ATRI (VE-821) for 0, 8, or 24 h. DNA fibers were treated with S1 nuclease, and the length of IdU tracts (*n* = 125 fibers per condition) was measured. One of two experiments is shown.

(B) U2OS cells transfected with control or UNG#1 siRNA and treated with 2 μ M ATRi (VE-821) for 48 h. 53BP1 nuclear bodies (NBs) in cyclin A-negative G1 cells were quantified (n > 1,200 cells per condition). One of two experiments is shown.

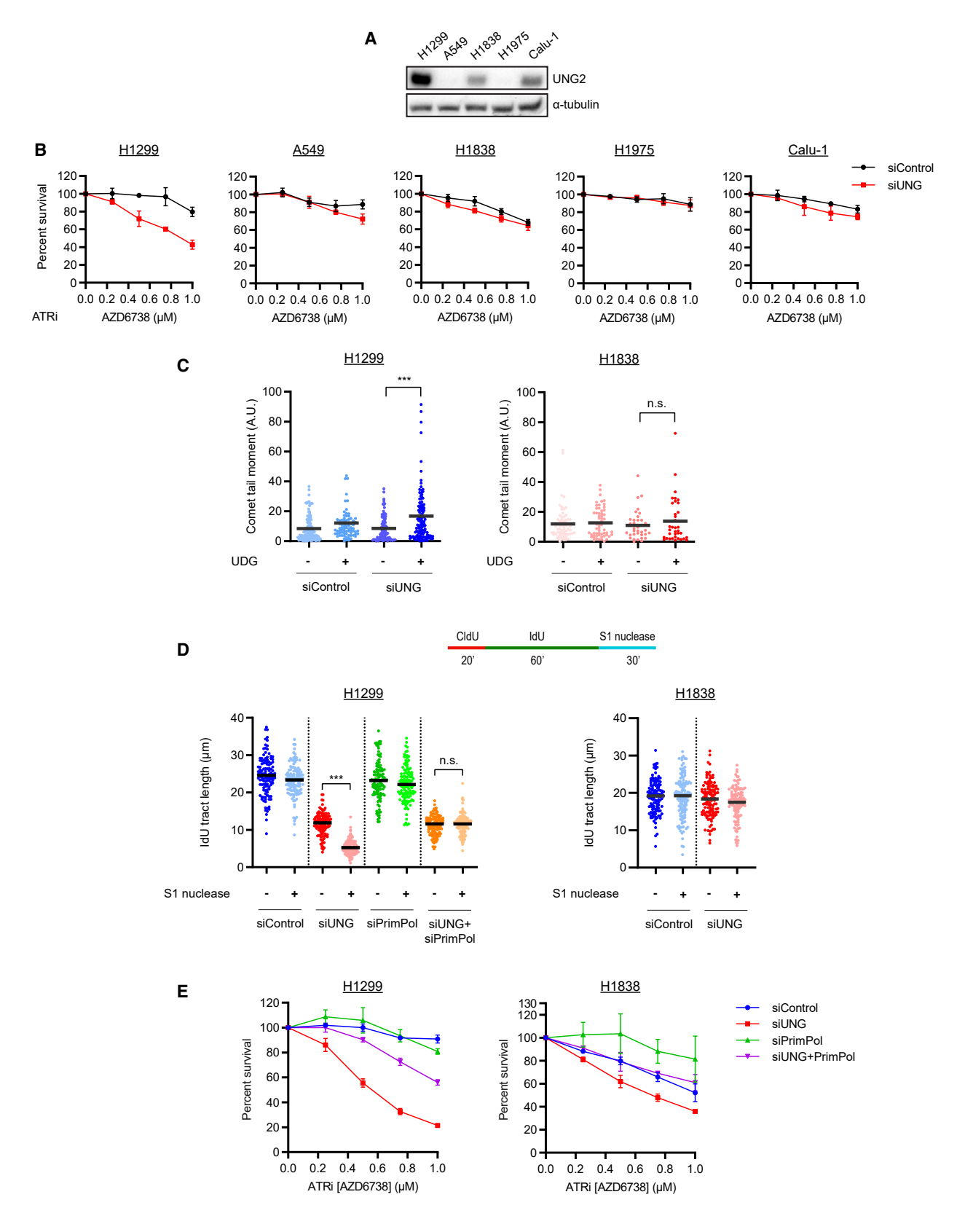
(C) Model for the induction of DNA damage by ATRi in cells lacking UNG2.

(D) U2OS cells were transfected with indicated siRNAs, labeled with 5 μ M EdU for 15 min, and then treated with 10 μ M ATRi (VE-821) for 24 h. γ H2AX intensity in EdU-positive cells was quantified (n > 250 cells per condition). One of two experiments is shown.

(E) U2OS cells were transfected with UNG#1, labeled with 5 μ M EdU for 15 min, then treated with 10 μ M ATRi (VE-821) +/- 10 μ M CDK1i (RO-3306) for 24 h, and analyzed as in (E) (n > 250 cells per condition). One of three experiments is shown.

(F) U2OS cells transfected with UNG#1 and PrimPol siRNA were treated and analyzed as in (D) (n > 250 cells per condition). One of three experiments is shown. (G) Viability of U2OS cells transfected with UNG#1 and PrimPol siRNA and treated with indicated concentrations of ATRi (VE-821). Data are shown as mean \pm SD. (n = 2 independent experiments).





(legend on next page)



Molecular Cell Article

also completely reversed the modest increase of ATRi sensitivity induced by UNG depletion (Figure 6E). Thus, in both H1299 and H1838, uracil-induced RS and ATRi sensitivity are largely attributed to PrimPol-generated ssDNA gaps. H1299, which is more dependent on UNG2 to suppress genomic uracil, is also more sensitive to ATRi upon UNG loss.

Induction of genomic uracil sensitizes UNG-dependent cancer cells to ATRi

Given our finding that some cancer cells are dependent on UNG2 to suppress genomic uracil and RS, we asked whether we could sensitize these cancer cells to ATRi by increasing genomic uracil without depleting UNG2. First, we knocked down dUTPase in H1299 and H1838 and tested the effects on ATRi sensitivity. dUTPase depletion increased ATRi sensitivity drastically in H1299 but only modestly in H1838 (Figure S7A). Next, we used PMX to increase genomic uracil in H1299 and H1838 cells. Remarkably, PMX significantly increased the ATRi sensitivity of H1299 cells but not H1838 cells (Figures 7A and S7B). Furthermore, PMX also drastically increased the ATRi sensitivity of HL-60, an AML cell line expressing UNG at high levels (Figure S7B) (Human Protein Atlas, proteinatlas.org). Importantly, the PMX-induced ATRi hypersensitivity of H1299 cells was completely reversed by thymidine (Figure 7B), confirming that PMX enhances ATRi sensitivity by reducing dTTP and increasing the dUTP/dTTP ratio. Together, these results suggest that PMX can be used to sensitize UNG-dependent cancer cells to ATRi.

Next, we asked whether the combination of ATRi and PMX is effective on UNG2-dependent tumors *in vivo*. We used H1299 cells to generate xenograft tumors in female non-obese diabetic (NOD) severe combined immunodeficiency (SCID) gamma (NSG) mice. Treatment with the ATRi AZD6738 or PMX alone delayed tumor growth as compared with DMSO controls (Figure 7C). Notably, a significantly higher anti-tumor effect was observed when ATRi and PMX were combined (Figures 7C and S7C). Neither ATRi nor PMX significantly reduced animal weights at the doses used (Figure S7D). Thus, the combination of ATRi and PMX is more effective than either drug alone in inhibiting the growth of tumors under uracil-induced RS *in vivo*.

Finally, we asked whether the findings from established lung cancer cell lines can be applied to patient-derived materials. We tested three cell lines derived from lung cancer patients at Massachusetts General Hospital (MGH). Among these lines, MGH707.1 and MGH134.1 expressed high levels of UNG2 protein, whereas UNG2 was undetected in MGH143.3B (Figure 7D). Consistent with the results from H1299 and H1838, knockdown of UNG significantly increased genomic uracil in MGH707.1 and

MGH134.1, but not in MGH143.3B (Figures S7E and S7F). Furthermore, UNG knockdown significantly reduced fork speed and increased ssDNA gaps in MGH707.1 and MGH134.1 (Figure S7G). By contrast, in MGH143.3B, UNG depletion only slightly reduced fork speed and did not significantly increase ssDNA gaps (Figure S7G). Importantly, PMX significantly sensitized MGH707.1 and MGH134.1, but not MGH143.3B, to ATRi (Figure 7D), showing that PMX effectively sensitizes patient-derived, UNG2-dependent tumor cells to ATRi.

DISCUSSION

Base alterations in the genome have been long appreciated to be a source of genomic instability. The increase of oxidative stress in cancer cells contributes to tumorigenesis in a variety of oncogenic contexts.⁵⁰ The induction of BER intermediates by oxidized bases (e.g., 8-oxoG) is believed to increase RS and ultimately give rise to DSBs,51 which may contribute to the cytotoxic effects of PARPi in BRCA1-deficient cells.⁵² Indeed, our experiments using OGG1i support this model (Figure 7E). Surprisingly, however, in contrast to this prevailing model, we also found that genomic uracil, a distinct type of base alteration, induces RS independently of UNG-mediated BER. In addition to UNG, we eliminated all known uracil glycosylases as backups for UNG to generate RS through BER intermediates, strengthening the notion that genomic uracil can induce RS independently of BER. In the absence of UNG2, the primary glycosylase that recognizes genomic uracil and initiates BER, replication forks slow down, and cells become increasingly sensitive to ATRi. These results suggest that unprocessed uracil in the genome impedes replication forks even more than the BER intermediates that it generates (Figure 7E). Although genomic uracil interferes with replication forks, our results do not exclude the possibility that uracil-induced BER intermediates also induce RS. The overall impact of genomic uracil on the genome is likely determined by the levels of uracil in DNA and the efficiency and kinetics of BER. If genomic uracil is abundant but does not trigger BER in a timely manner, unprocessed uracil is probably the predominant source of RS. By contrast, if BER is initiated but not completed properly, genomic uracil may induce RS through BER intermediates. It is conceivable that genomic uracil can induce RS in both BER-independent and -dependent manners, and the contributions of these mechanisms may vary in cancer cells depending on the levels of genomic uracil and the status of the BER pathway. Notably, recent studies showed that loss of SMUG1 reduced the sensitivity of BRCA1-deficient cells to PARPi, 14,43 suggesting that AP sites are more toxic than

Figure 6. A subset of cancer cells relies on UNG2 to suppress replication stress

(A) Levels of UNG2 in the indicated cell lines. α -Tubulin serves as a loading control.

⁽B) The indicated cell lines were transfected with control or UNG#1 siRNA and treated with indicated concentrations of ATRi (AZD6738). Cell viability was analyzed with CellTiter-Glo in 5–7 days. Data are shown as mean ± SD. (n = 4 independent experiments).

⁽C) H1299 and H1838 cells transfected with control or UNG#1 siRNA were analyzed by U-comet assay (n > 50 cells per condition). One of two experiments is shown.

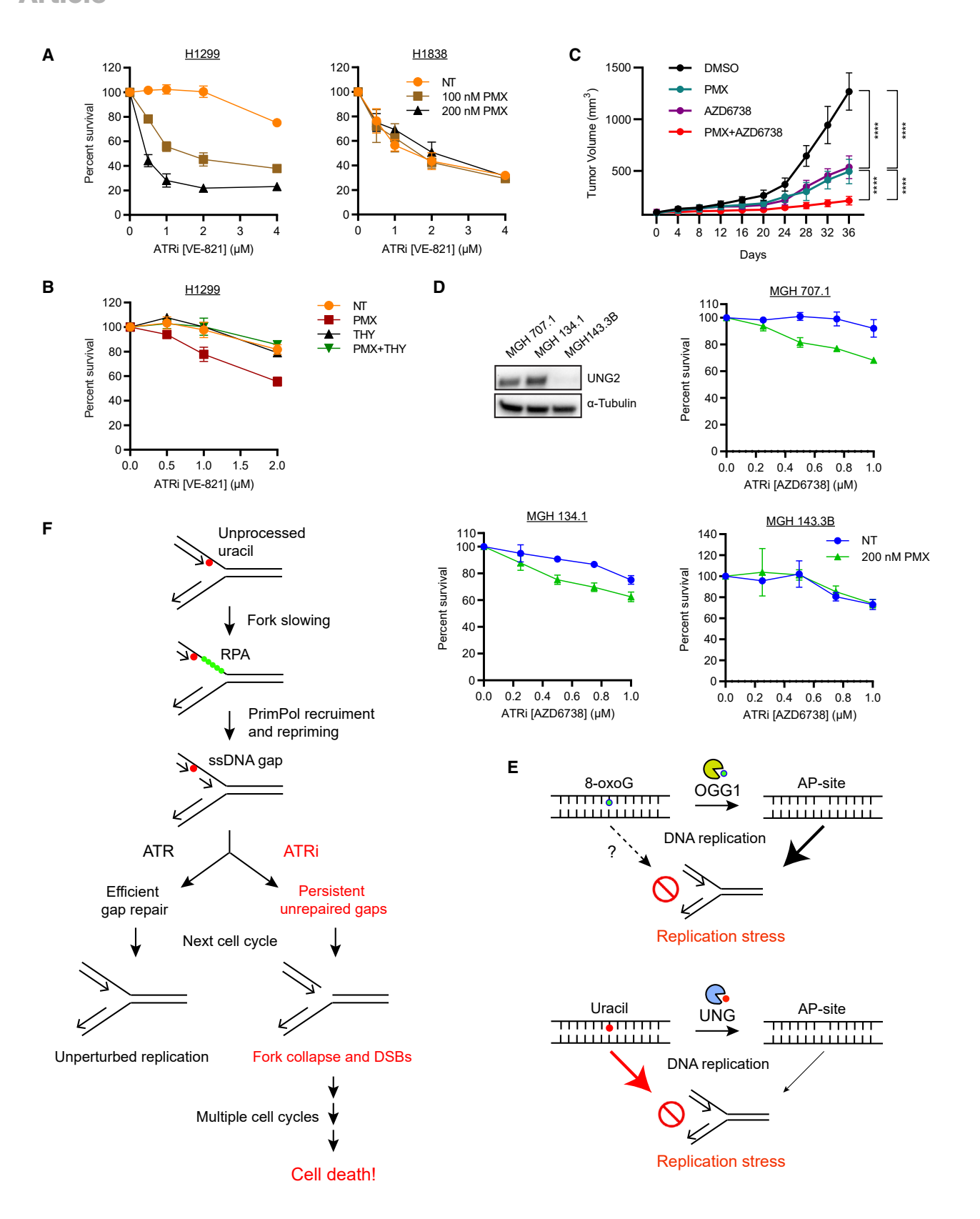
⁽D) H1299 and H1838 cells were transfected with control or UNG#1 and PrimPol siRNAs for 48 h. DNA fibers were treated with S1 nuclease, and the length of IdU tracts (n = 125 fibers per condition) was measured. One of two experiments is shown.

⁽E) Viability of H1299 and H1838 cells transfected with UNG#1 and PrimPol siRNA and treated with indicated concentrations of ATRi (AZD6738). Data are shown as mean ± SD. (n = 2 independent experiments).

Molecular Cell

Article





(legend on next page)



unprocessed hmdU in the context of BRCA1 deficiency and PARP trapping. This finding provides a possible example of how the genetic background of cancer cells and the action of cancer drugs may influence the effects of uracil and its derivatives in the genome.

In this study, we unexpectedly found that genomic uracil slows down replication forks. This slowdown of replication forks is independent of UNG, suggesting that unprocessed genomic uracil is responsible. Importantly, our PLA analysis using RPA32 and Pole catalytic subunit antibodies suggests that Polε is uncoupled from the replicative helicase by genomic uracil in human cells, which is a predicted effect of polymerase slowdown. Furthermore, our in vitro biochemical experiments show that purified hPole exo is stalled by dU on template DNA, providing direct evidence for the impediment of DNA synthesis by unprocessed uracil. Thus, although previous biochemical studies did not detect a slowdown of yeast DNA polymerases on dU-containing DNA templates,53 our results suggest that genomic uracil impedes human DNA Polε and interferes with DNA replication in human cells. During DNA synthesis, the dU in template DNA may generate base pairs that are recognized by the proofreading domain of $\mathsf{Pol}\epsilon$ as mismatches, thus triggering editing by the exonuclease domain and polymerase pausing. This pausing may be particularly prominent for hPolε exo- because it lacks the critical residues required for the exonuclease activity.

Our experiments also reveal that genomic uracil increases PrimPol-mediated repriming at replication forks, an event triggered by the accumulation of ssDNA and RPA ahead of DNA polymerases. Although PrimPol-mediated repriming allows replication forks to progress through the uracil in template, it generates ssDNA gaps that can subsequently give rise to DSBs. Notably, ATRi prevents the efficient repair of uracilinduced gaps. The inhibition of gap repair by ATRi makes these gaps more persistent, leading to fork collapse in the next S phase (Figure 7F). ATRi also inhibits the repair of collapsed forks, making cancer cells under uracil stress even more dependent on ATR for survival. The trapping of PARP1/2 by PARPi also prevents efficient gap repair. 42,54,55 Furthermore, recent studies implicated both TLS and POLQ in the repair of ssDNA gaps. 44,48,56,57 Indeed, we found that TLS is critical for the repair of uracil-induced ssDNA gaps. It is possible that inhibitors of PARP1/2, TLS, and POLQ can preferentially kill cancer cells under high levels of uracil-associated RS.

What types of cancer cells harbor high levels of genomic uracil? The balance of dUTP and dTTP in cancer cells is likely a key determinant of the frequency of uracil misincorporation and

genomic uracil levels. 18 Supporting this notion, PMX increases the dUTP/dTTP ratio and elevates genomic uracil levels in cancer cells.⁵⁸ It is possible that alternations of a number of metabolic pathways in cancer cells increase the dUTP/dTTP ratio and promote the accumulation of uracil in the genome. Furthermore, the cytidine deamination by AID or APOBEC is likely another source of genomic uracil in cancer cells. 17,59 Of note, our recent work shows that expression of APOBEC3A also induces PrimPol-generated ssDNA gaps, which confers ATRi sensitivity. 60 When cancer cells harbor high levels of genomic uracil, they have to cope with uracil-induced RS by limiting genomic uracil and activating the RS response. Both upregulation of BER and metabolic changes reducing the dUTP/dTTP ratio could be used by cancer cells to limit genomic uracil. For example, human lung cancer cells upregulate UNG in response to PMX exposure. 49 Cancer cells also use thymidylate kinase (TMPK) to prevent dUTP incorporation during DNA repair. 61 We found that cancer cells expressing high levels of UNG2 are more dependent on UNG to suppress genomic uracil. This addiction of cancer cells to suppressors of genomic uracil creates an opportunity to exploit uracil-induced RS. The leukemia cell line HL-60, which expresses high levels of UNG, is sensitive to MTHFD2 inhibitors, which reduce thymidine synthesis and increase genomic uracil. 62 Drugs such as PMX or dUTPase inhibitors can also be used to exacerbate the uracil-induced RS in cancer cells. Furthermore, when uracil-induced RS is exacerbated in cancer cells, they become even more dependent on ATR-mediated gap repair and the RS response for survival. This model provides a rationale to target cancer cells under high uracil stress using combinations of ATRi with PMX, dUT-Pase inhibitors, or MTHFD2 inhibitors. In future studies, it is important to identify biomarkers for tumors harboring high uracil stress and develop therapeutics to effectively exacerbate and exploit the uracil-induced RS.

Limitations of the study

It should be noted that hPol ϵ exo $^-$ but not full-length hPol ϵ was used in our biochemical experiments. The extent to which full-length hPol ϵ is slowed by genomic uracil still needs to be tested. Although our results show that several cancer cell lines expressing high levels of UNG2 are sensitive to ATRi upon UNG depletion, high UNG2 expression alone is unlikely sufficient to broadly predict uracil-induced RS in cancer cells. Mechanisms other than UNG2 upregulation may also be used by cancer cells to cope with uracil-induced RS. To reliably identify tumors under high uracil-induced RS, additional biomarkers and/or clinical assays need to be developed in future studies.

Figure 7. Induction of genomic uracil sensitizes UNG-dependent cancer cells to ATRi

(A) Viability of H1299 and H1838 cells treated with indicated concentrations of PMX and ATRi (VE-821). Data are shown as mean ± SD. (n = 2 independent experiments).

(B) Viability of H1299 cells treated with 100 nM PMX, 50 μM THY, and indicated concentrations of ATRi (VE-821) (n = 2 independent experiments).

(C) Growth curves of H1299 tumors in control mice and mice treated with 50 mg/kg ATRi (AZD6738) and/or 75 mg/kg PMX. n = 4 mice in each group. Two-way ANOVA with Tukey's multiple comparisons test was used to measure the significance throughout. (ns) non-significant; $p \le 0.05$; ** $p \le 0.01$; ** $p \le 0.01$.

(D) Viability of MGH 707.1, MGH 134.1, and MGH 143-3B cells treated with 200 nM PMX and indicated concentrations of ATRi (AZD6738) (n = 2 independent experiments). Levels of UNG2 in the indicated cells were analyzed by western blot. α-Tubulin serves as a loading control.

(E) Model for RS induction by different types of base lesions.

(F) Model for RS induction by unprocessed uracil and the effects in the presence and absence of ATRi.

Molecular Cell

Article



STAR*METHODS

Detailed methods are provided in the online version of this paper and include the following:

- KEY RESOURCES TABLE
- RESOURCE AVAILABILITY
 - Lead contact
 - Materials availability
 - Data and code availability
- EXPERIMENTAL MODEL AND STUDY PARTICIPANT DETAILS
 - Cell culture
- METHOD DETAILS
 - Cloning
 - o CRISPR-Cas9 KO cell lines
 - Plasmid transfection
 - o RNA interference
 - O Quantitative real-time PCR
 - Measurement of AP sites
 - U-comet assay
 - High-performance liquid chromatography-mass spectrometry measurement of genomic deoxyuridine
 - O DNA fiber analysis
 - Uracil excision activity assay
 - Import of dNTPs into live cells
 - o Immunofluorescence
 - Proximity ligation assay
 - Immunoblots
 - Chromatin fractionation
 - o Primer extension assay
 - Cell viability assay
 - o In vivo drug response
- QUANTIFICATION AND STATISTICAL ANALYSIS

SUPPLEMENTAL INFORMATION

Supplemental information can be found online at https://doi.org/10.1016/j.molcel.2024.04.004.

ACKNOWLEDGMENTS

We thank members of Zou, Dyson, Lan, Mostoslavsky, Elia, and Motamedi labs for helpful discussions; Dr. M. Lawrence for bioinformatic analysis; Dr. C. Ott and the MGH Center for Molecular Therapeutics for cell lines; and M. Basu for help with RT-qPCR. We acknowledge communications with Dr. C. Bakkenist, whose independent data also implicates uracil in replication stress. S.S. was supported by the James A. Harting Scientific Scholar Award from the Rivkin Center. P.S.P. is a Banting fellow. L.Z. was the James and Patricia Poitras Endowed Chair in Cancer Research. This work is supported by the NIH grants CA248526 and CA263934 to L.Z., GM122093 to Z.S., GM146933 to E.O., the NSF grant MCB-1716168 to Z.S., and funding from the Lungstrong Foundation to A.N.H. The graphical abstract was created with BioRender.com.

AUTHOR CONTRIBUTIONS

S.S. and L.Z. designed the study with inputs from other authors. S.S. performed the majority of the experiments and data analysis. C.S.N. and C.R.C. performed the LC-MS experiments. P.S.P. performed the mouse experiment. T.W.S. and H.T. performed the primer extension assays. A.S.K. performed the uracil glycosylase assays. E.O., M.G.V.H., Z.S., and L.Z. supervised the study. A.N.H. provided critical reagents. S.S. and L.Z. wrote the manuscript with inputs from all authors.

DECLARATION OF INTERESTS

The authors declare no competing interests with this study. L.Z. is a member of the advisory board of *Molecular Cell*, a scientific advisor for Sirrona Therapeu-

tics, and received research support from Calico, Pfizer, and Bristol Myers Squibb. A.N.H. received research support from Amgen, Blueprint Medicines, BridgeBio, Bristol-Myers Squibb, C4 Therapeutics, Eli Lilly, Novartis, Nuvalent, Pfizer, Roche/Genentech, and Scorpion Therapeutics and consulted for Engine Biosciences, Oncovalent, Nuvalent, TigaTx, and Tolremo Therapeutics. M.G.V.H. is a scientific advisor for Agios Pharmaceuticals, iTeos Therapeutics, Sage Therapeutics, Auron Therapeutics, and Droia Ventures.

Received: May 16, 2023 Revised: March 26, 2024 Accepted: April 5, 2024 Published: April 29, 2024

REFERENCES

- Saxena, S., and Zou, L. (2022). Hallmarks of DNA replication stress. Mol. Cell 82, 2298–2314. https://doi.org/10.1016/j.molcel.2022.05.004.
- Zeman, M.K., and Cimprich, K.A. (2014). Causes and consequences of replication stress. Nat. Cell Biol. 16, 2–9. https://doi.org/10.1038/ nch2897
- da Costa, A.A.B.A., Chowdhury, D., Shapiro, G.I., D'Andrea, A.D., and Konstantinopoulos, P.A. (2023). Targeting replication stress in cancer therapy. Nat. Rev. Drug Discov. 22, 38–58. https://doi.org/10.1038/s41573-022-00558-5.
- Hopkins, J.L., Lan, L., and Zou, L. (2022). DNA repair defects in cancer and therapeutic opportunities. Genes Dev. 36, 278–293. https://doi.org/10. 1101/gad.349431.122.
- Kotsantis, P., Petermann, E., and Boulton, S.J. (2018). Mechanisms of Oncogene-Induced Replication Stress: Jigsaw Falling into Place. Cancer Discov. 8, 537–555. https://doi.org/10.1158/2159-8290.CD-17-1461.
- Macheret, M., and Halazonetis, T.D. (2015). DNA replication stress as a hallmark of cancer. Annu. Rev. Pathol. 10, 425–448. https://doi.org/10. 1146/annurev-pathol-012414-040424.
- Brickner, J.R., Garzon, J.L., and Cimprich, K.A. (2022). Walking a tightrope: The complex balancing act of R-loops in genome stability. Mol. Cell 82, 2267–2297. https://doi.org/10.1016/j.molcel.2022.04.014.
- Cortez, D. (2019). Replication-Coupled DNA Repair. Mol. Cell 74, 866–876. https://doi.org/10.1016/j.molcel.2019.04.027.
- Petermann, E., Lan, L., and Zou, L. (2022). Sources, resolution and physiological relevance of R-loops and RNA-DNA hybrids. Nat. Rev. Mol. Cell Biol. 23, 521–540. https://doi.org/10.1038/s41580-022-00474-x.
- Pai, C.C., and Kearsey, S.E. (2017). A Critical Balance: dNTPs and the Maintenance of Genome Stability. Genes (Basel) 8, 57. https://doi.org/ 10.3390/genes8020057.
- Bauer, C., Göbel, K., Nagaraj, N., Colantuoni, C., Wang, M., Müller, U., Kremmer, E., Rottach, A., and Leonhardt, H. (2015). Phosphorylation of TET proteins is regulated via O-GlcNAcylation by the O-linked N-acetylglucosamine transferase (OGT). J. Biol. Chem. 290, 4801– 4812. https://doi.org/10.1074/jbc.M114.605881.
- Caldecott, K.W. (2020). Mammalian DNA base excision repair: dancing in the moonlight. DNA Repair (Amst) 93, 102921. https://doi.org/10.1016/j. dnarep.2020.102921.
- Thompson, P.S., and Cortez, D. (2020). New insights into abasic site repair and tolerance. DNA Repair (Amst) 90, 102866. https://doi.org/10.1016/j. dnarep.2020.102866.
- Fugger, K., Bajrami, I., Silva Dos Santos, M., Young, S.J., Kunzelmann, S., Kelly, G., Hewitt, G., Patel, H., Goldstone, R., Carell, T., et al. (2021). Targeting the nucleotide salvage factor DNPH1 sensitizes BRCA-deficient cells to PARP inhibitors. Science 372, 156–165. https://doi.org/10.1126/ science.abb4542.
- Szatrowski, T.P., and Nathan, C.F. (1991). Production of large amounts of hydrogen peroxide by human tumor cells. Cancer Res. 51, 794–798.
- Petljak, M., Dananberg, A., Chu, K., Bergstrom, E.N., Striepen, J., von Morgen, P., Chen, Y., Shah, H., Sale, J.E., Alexandrov, L.B., et al. (2022).



- Mechanisms of APOBEC3 mutagenesis in human cancer cells. Nature 607, 799–807. https://doi.org/10.1038/s41586-022-04972-y.
- Pettersen, H.S., Galashevskaya, A., Doseth, B., Sousa, M.M., Sarno, A., Visnes, T., Aas, P.A., Liabakk, N.B., Slupphaug, G., Sætrom, P., et al. (2015). AID expression in B-cell lymphomas causes accumulation of genomic uracil and a distinct AID mutational signature. DNA Repair (Amst) 25, 60–71. https://doi.org/10.1016/j.dnarep.2014.11.006.
- Berger, S.H., Pittman, D.L., and Wyatt, M.D. (2008). Uracil in DNA: consequences for carcinogenesis and chemotherapy. Biochem. Pharmacol. 76, 697–706. https://doi.org/10.1016/j.bcp.2008.05.019.
- Saldivar, J.C., Cortez, D., and Cimprich, K.A. (2017). The essential kinase ATR: ensuring faithful duplication of a challenging genome. Nat. Rev. Mol. Cell Biol. 18, 622–636. https://doi.org/10.1038/nrm.2017.67.
- Zou, L., and Elledge, S.J. (2003). Sensing DNA damage through ATRIP recognition of RPA-ssDNA complexes. Science 300, 1542–1548. https://doi.org/10.1126/science.1083430.
- Konstantinopoulos, P.A., da Costa, A.A.B.A., Gulhan, D., Lee, E.K., Cheng, S.C., Hendrickson, A.E.W., Kochupurakkal, B., Kolin, D.L., Kohn, E.C., Liu, J.F., et al. (2021). A Replication stress biomarker is associated with response to gemcitabine versus combined gemcitabine and ATR inhibitor therapy in ovarian cancer. Nat. Commun. 12, 5574. https://doi.org/ 10.1038/s41467-021-25904-w.
- Thomas, A., Takahashi, N., Rajapakse, V.N., Zhang, X., Sun, Y., Ceribelli, M., Wilson, K.M., Zhang, Y., Beck, E., Sciuto, L., et al. (2021). Therapeutic targeting of ATR yields durable regressions in small cell lung cancers with high replication stress. Cancer Cell 39, 566–579.e7. https://doi.org/10. 1016/j.ccell.2021.02.014.
- Visnes, T., Cázares-Körner, A., Hao, W., Wallner, O., Masuyer, G., Loseva, O., Mortusewicz, O., Wiita, E., Sarno, A., Manoilov, A., et al. (2018). Small-molecule inhibitor of OGG1 suppresses proinflammatory gene expression and inflammation. Science 362, 834–839. https://doi.org/10.1126/science.aar8048.
- Krokan, H.E., Drabløs, F., and Slupphaug, G. (2002). Uracil in DNA-occurrence, consequences and repair. Oncogene 21, 8935–8948. https://doi.org/10.1038/sj.onc.1205996.
- Visnes, T., Doseth, B., Pettersen, H.S., Hagen, L., Sousa, M.M., Akbari, M., Otterlei, M., Kavli, B., Slupphaug, G., and Krokan, H.E. (2009).
 Uracil in DNA and its processing by different DNA glycosylases. Philos. Trans. R. Soc. Lond. B Biol. Sci. 364, 563–568. https://doi.org/10.1098/rstb.2008.0186.
- Kemmerich, K., Dingler, F.A., Rada, C., and Neuberger, M.S. (2012).
 Germline ablation of SMUG1 DNA glycosylase causes loss of 5-hydroxymethyluracil- and UNG-backup uracil-excision activities and increases cancer predisposition of Ung-/-Msh2-/- mice. Nucleic Acids Res. 40, 6016–6025. https://doi.org/10.1093/nar/gks259.
- Sjolund, A.B., Senejani, A.G., and Sweasy, J.B. (2013). MBD4 and TDG: multifaceted DNA glycosylases with ever expanding biological roles. Mutat. Res. 12–25. 743–744. https://doi.org/10.1016/j.mrfmmm.2012. 11.001.
- 28. Shih, C., Chen, V.J., Gossett, L.S., Gates, S.B., MacKellar, W.C., Habeck, L.L., Shackelford, K.A., Mendelsohn, L.G., Soose, D.J., Patel, V.F., et al. (1997). LY231514, a pyrrolo[2,3-d]pyrimidine-based antifolate that inhibits multiple folate-requiring enzymes. Cancer Res. 57, 1116–1123.
- Bjursell, G., and Reichard, P. (1973). Effects of thymidine on deoxyribonucleoside triphosphate pools and deoxyribonucleic acid synthesis in Chinese hamster ovary cells. J. Biol. Chem. 248, 3904–3909.
- Ladner, R.D., McNulty, D.E., Carr, S.A., Roberts, G.D., and Caradonna, S.J. (1996). Characterization of distinct nuclear and mitochondrial forms of human deoxyuridine triphosphate nucleotidohydrolase. J. Biol. Chem. 271, 7745–7751. https://doi.org/10.1074/jbc.271.13.7745.
- Yokogawa, T., Yano, W., Tsukioka, S., Osada, A., Wakasa, T., Ueno, H., Hoshino, T., Yamamura, K., Fujioka, A., Fukuoka, M., et al. (2021). dUTPase inhibition confers susceptibility to a thymidylate synthase inhib-

- itor in DNA-repair-defective human cancer cells. Cancer Sci. 112, 422–432. https://doi.org/10.1111/cas.14718.
- Bermudez, V.P., Farina, A., Raghavan, V., Tappin, I., and Hurwitz, J. (2011). Studies on human DNA polymerase epsilon and GINS complex and their role in DNA replication. J. Biol. Chem. 286, 28963–28977. https://doi.org/10.1074/jbc.M111.256289.
- Korona, D.A., Lecompte, K.G., and Pursell, Z.F. (2011). The high fidelity and unique error signature of human DNA polymerase epsilon. Nucleic Acids Res. 39, 1763–1773. https://doi.org/10.1093/nar/gkq1034.
- Zahurancik, W.J., Baranovskiy, A.G., Tahirov, T.H., and Suo, Z. (2015).
 Comparison of the kinetic parameters of the truncated catalytic subunit and holoenzyme of human DNA polymerase ε. DNA Repair (Amst) 29, 16–22. https://doi.org/10.1016/j.dnarep.2015.01.008.
- Zahurancik, W.J., Klein, S.J., and Suo, Z. (2013). Kinetic mechanism of DNA polymerization catalyzed by human DNA polymerase epsilon. Biochemistry 52, 7041–7049. https://doi.org/10.1021/bi400803v.
- Byun, T.S., Pacek, M., Yee, M.C., Walter, J.C., and Cimprich, K.A. (2005). Functional uncoupling of MCM helicase and DNA polymerase activities activates the ATR-dependent checkpoint. Genes Dev. 19, 1040–1052. https://doi.org/10.1101/gad.1301205.
- Guilliam, T.A., Brissett, N.C., Ehlinger, A., Keen, B.A., Kolesar, P., Taylor, E.M., Bailey, L.J., Lindsay, H.D., Chazin, W.J., and Doherty, A.J. (2017). Molecular basis for PrimPol recruitment to replication forks by RPA. Nat. Commun. 8, 15222. https://doi.org/10.1038/ncomms15222.
- Bianchi, J., Rudd, S.G., Jozwiakowski, S.K., Bailey, L.J., Soura, V., Taylor, E., Stevanovic, I., Green, A.J., Stracker, T.H., Lindsay, H.D., and Doherty, A.J. (2013). PrimPol bypasses UV photoproducts during eukaryotic chromosomal DNA replication. Mol. Cell 52, 566–573. https://doi.org/10.1016/ j.molcel.2013.10.035.
- Mourón, S., Rodriguez-Acebes, S., Martínez-Jiménez, M.I., García-Gómez, S., Chocrón, S., Blanco, L., and Méndez, J. (2013). Repriming of DNA synthesis at stalled replication forks by human PrimPol. Nat. Struct. Mol. Biol. 20, 1383–1389. https://doi.org/10.1038/nsmb.2719.
- Quinet, A., Carvajal-Maldonado, D., Lemacon, D., and Vindigni, A. (2017).
 DNA Fiber Analysis: Mind the Gap! Methods Enzymol. 591, 55–82. https://doi.org/10.1016/bs.mie.2017.03.019.
- Zawada, Z., Tatar, A., Mocilac, P., Buděšínský, M., and Kraus, T. (2018).
 Transport of Nucleoside Triphosphates into Cells by Artificial Molecular Transporters. Angew. Chem. Int. Ed. Engl. 57, 9891–9895. https://doi. org/10.1002/anie.201801306.
- Simoneau, A., Xiong, R., and Zou, L. (2021). The trans cell cycle effects of PARP inhibitors underlie their selectivity toward BRCA1/2-deficient cells. Genes Dev. 35, 1271–1289. https://doi.org/10.1101/gad.348479.121.
- Taglialatela, A., Leuzzi, G., Sannino, V., Cuella-Martin, R., Huang, J.W., Wu-Baer, F., Baer, R., Costanzo, V., and Ciccia, A. (2021). REV1-Polζ maintains the viability of homologous recombination-deficient cancer cells through mutagenic repair of PRIMPOL-dependent ssDNA gaps. Mol. Cell 81, 4008–4025.e7. https://doi.org/10.1016/j.molcel.2021.08.016.
- 44. Tirman, S., Quinet, A., Wood, M., Meroni, A., Cybulla, E., Jackson, J., Pegoraro, S., Simoneau, A., Zou, L., and Vindigni, A. (2021). Temporally distinct post-replicative repair mechanisms fill PRIMPOL-dependent ssDNA gaps in human cells. Mol. Cell 81, 4026–4040.e8. https://doi.org/10.1016/j.molcel.2021.09.013.
- Harrigan, J.A., Belotserkovskaya, R., Coates, J., Dimitrova, D.S., Polo, S.E., Bradshaw, C.R., Fraser, P., and Jackson, S.P. (2011). Replication stress induces 53BP1-containing OPT domains in G1 cells. J. Cell Biol. 193. 97–108. https://doi.org/10.1083/icb.201011083.
- Lukas, C., Savic, V., Bekker-Jensen, S., Doil, C., Neumann, B., Pedersen, R.S., Grøfte, M., Chan, K.L., Hickson, I.D., Bartek, J., and Lukas, J. (2011).
 53BP1 nuclear bodies form around DNA lesions generated by mitotic transmission of chromosomes under replication stress. Nat. Cell Biol. 13, 243–253. https://doi.org/10.1038/ncb2201.

Molecular Cell

Article



- Regairaz, M., Zhang, Y.W., Fu, H., Agama, K.K., Tata, N., Agrawal, S., Aladjem, M.I., and Pommier, Y. (2011). Mus81-mediated DNA cleavage resolves replication forks stalled by topoisomerase I-DNA complexes. J. Cell Biol. 195, 739–749. https://doi.org/10.1083/jcb.201104003.
- Mann, A., Ramirez-Otero, M.A., De Antoni, A., Hanthi, Y.W., Sannino, V., Baldi, G., Falbo, L., Schrempf, A., Bernardo, S., Loizou, J., and Costanzo, V. (2022). POLθ prevents MRE11-NBS1-CtIP-dependent fork breakage in the absence of BRCA2/RAD51 by filling lagging-strand gaps. Mol. Cell 82, 4218–4231.e8. https://doi.org/10.1016/j.molcel.2022. 09.013.
- Weeks, L.D., Fu, P., and Gerson, S.L. (2013). Uracil-DNA glycosylase expression determines human lung cancer cell sensitivity to pemetrexed. Mol. Cancer Ther. 12, 2248–2260. https://doi.org/10.1158/1535-7163. MCT-13-0172.
- Hayes, J.D., Dinkova-Kostova, A.T., and Tew, K.D. (2020). Oxidative Stress in Cancer. Cancer Cell 38, 167–197. https://doi.org/10.1016/j. ccell.2020.06.001.
- Mohni, K.N., Wessel, S.R., Zhao, R., Wojciechowski, A.C., Luzwick, J.W., Layden, H., Eichman, B.F., Thompson, P.S., Mehta, K.P.M., and Cortez, D. (2019). HMCES Maintains Genome Integrity by Shielding Abasic Sites in Single-Strand DNA. Cell 176, 144–153.e13. https://doi.org/10.1016/j. cell.2018.10.055.
- Giovannini, S., Weller, M.C., Repmann, S., Moch, H., and Jiricny, J. (2019). Synthetic lethality between BRCA1 deficiency and poly(ADP-ribose) polymerase inhibition is modulated by processing of endogenous oxidative DNA damage. Nucleic Acids Res. 47, 9132–9143. https://doi.org/10.1093/nar/gkz624.
- Wardle, J., Burgers, P.M., Cann, I.K., Darley, K., Heslop, P., Johansson, E., Lin, L.J., McGlynn, P., Sanvoisin, J., Stith, C.M., and Connolly, B.A. (2008).
 Uracil recognition by replicative DNA polymerases is limited to the archaea, not occurring with bacteria and eukarya. Nucleic Acids Res. 36, 705–711. https://doi.org/10.1093/nar/gkm1023.
- Vaitsiankova, A., Burdova, K., Sobol, M., Gautam, A., Benada, O., Hanzlikova, H., and Caldecott, K.W. (2022). PARP inhibition impedes the maturation of nascent DNA strands during DNA replication. Nat. Struct. Mol. Biol. 29, 329–338. https://doi.org/10.1038/s41594-022-00747-1.
- Cong, K., Peng, M., Kousholt, A.N., Lee, W.T.C., Lee, S., Nayak, S., Krais, J., VanderVere-Carozza, P.S., Pawelczak, K.S., Calvo, J., et al. (2021). Replication gaps are a key determinant of PARP inhibitor synthetic lethality with BRCA deficiency. Mol. Cell 81, 3128–3144.e7. https://doi.org/10. 1016/j.molcel.2021.06.011.
- Belan, O., Sebald, M., Adamowicz, M., Anand, R., Vancevska, A., Neves, J., Grinkevich, V., Hewitt, G., Segura-Bayona, S., Bellelli, R., et al. (2022).
 POLQ seals post-replicative ssDNA gaps to maintain genome stability in BRCA-deficient cancer cells. Mol. Cell 82, 4664–4680.e9. https://doi. org/10.1016/j.molcel.2022.11.008.
- Schrempf, A., Bernardo, S., Arasa Verge, E.A., Ramirez Otero, M.A., Wilson, J., Kirchhofer, D., Timelthaler, G., Ambros, A.M., Kaya, A., Wieder, M., et al. (2022). POLθ processes ssDNA gaps and promotes replication fork progression in BRCA1-deficient cells. Cell Rep. 41, 111716. https://doi.org/10.1016/j.celrep.2022.111716.
- Bulgar, A.D., Weeks, L.D., Miao, Y., Yang, S., Xu, Y., Guo, C., Markowitz, S., Oleinick, N., Gerson, S.L., and Liu, L. (2012). Removal of uracil by uracil DNA glycosylase limits pemetrexed cytotoxicity: overriding the limit with methoxyamine to inhibit base excision repair. Cell Death Dis. 3, e252. https://doi.org/10.1038/cddis.2011.135.
- Petljak, M., and Maciejowski, J. (2020). Molecular origins of APOBECassociated mutations in cancer. DNA Repair (Amst) 94, 102905. https:// doi.org/10.1016/j.dnarep.2020.102905.
- Kawale, A.S., Ran, X., Patel, P.S., Saxena, S., Lawrence, M.S., and Zou, L. (2024). APOBEC3A induces DNA gaps through PRIMPOL and confers

- gap-associated therapeutic vulnerability. Sci. Adv. 10, eadk2771. https://doi.org/10.1126/sciadv.adk2771.
- Hu, C.M., Yeh, M.T., Tsao, N., Chen, C.W., Gao, Q.Z., Chang, C.Y., Lee, M.H., Fang, J.M., Sheu, S.Y., Lin, C.J., et al. (2012). Tumor cells require thymidylate kinase to prevent dUTP incorporation during DNA repair. Cancer Cell 22, 36–50. https://doi.org/10.1016/j.ccr.2012.04.038.
- 62. Bonagas, N., Gustafsson, N.M.S., Henriksson, M., Marttila, P., Gustafsson, R., Wiita, E., Borhade, S., Green, A.C., Vallin, K.S.A., Sarno, A., et al. (2022). Pharmacological targeting of MTHFD2 suppresses acute myeloid leukemia by inducing thymidine depletion and replication stress. Nat. Cancer 3, 156–172. https://doi.org/10.1038/s43018-022-00331-y.
- Dash, R.C., Ozen, Z., Rizzo, A.A., Lim, S., Korzhnev, D.M., and Hadden, M.K. (2018). Structural Approach To Identify a Lead Scaffold That Targets the Translesion Synthesis Polymerase Rev1. J. Chem. Inf. Model. 58, 2266–2277. https://doi.org/10.1021/acs.jcim.8b00535.
- 64. Stanzione, M., Zhong, J., Wong, E., LaSalle, T.J., Wise, J.F., Simoneau, A., Myers, D.T., Phat, S., Sade-Feldman, M., Lawrence, M.S., et al. (2022). Translesion DNA synthesis mediates acquired resistance to olaparib plus temozolomide in small cell lung cancer. Sci. Adv. 8, eabn1229. https://doi.org/10.1126/sciadv.abn1229.
- Meerbrey, K.L., Hu, G., Kessler, J.D., Roarty, K., Li, M.Z., Fang, J.E., Herschkowitz, J.I., Burrows, A.E., Ciccia, A., Sun, T., et al. (2011). The pINDUCER lentiviral toolkit for inducible RNA interference *in vitro* and *in vivo*. Proc. Natl. Acad. Sci. U S A *108*, 3665–3670. https://doi.org/10. 1073/pnas.1019736108.
- Raoof, S., Mulford, I.J., Frisco-Cabanos, H., Nangia, V., Timonina, D., Labrot, E., Hafeez, N., Bilton, S.J., Drier, Y., Ji, F., et al. (2019). Targeting FGFR overcomes EMT-mediated resistance in EGFR mutant non-small cell lung cancer. Oncogene 38, 6399–6413. https://doi.org/10. 1038/s41388-019-0887-2.
- 67. Crystal, A.S., Shaw, A.T., Sequist, L.V., Friboulet, L., Niederst, M.J., Lockerman, E.L., Frias, R.L., Gainor, J.F., Amzallag, A., Greninger, P., et al. (2014). Patient-derived models of acquired resistance can identify effective drug combinations for cancer. Science 346, 1480–1486. https://doi.org/10.1126/science.1254721.
- Hata, A.N., Niederst, M.J., Archibald, H.L., Gomez-Caraballo, M., Siddiqui, F.M., Mulvey, H.E., Maruvka, Y.E., Ji, F., Bhang, H.E., Krishnamurthy Radhakrishna, V., et al. (2016). Tumor cells can follow distinct evolutionary paths to become resistant to epidermal growth factor receptor inhibition. Nat. Med. 22, 262–269. https://doi.org/10.1038/ pp. 4040.
- Kodack, D.P., Farago, A.F., Dastur, A., Held, M.A., Dardaei, L., Friboulet, L., von Flotow, F., Damon, L.J., Lee, D., Parks, M., et al. (2017). Primary Patient-Derived Cancer Cells and Their Potential for Personalized Cancer Patient Care. Cell Rep. 21, 3298–3309. https://doi.org/10.1016/j. celrep.2017.11.051.
- Sarno, A., Lundbæk, M., Liabakk, N.B., Aas, P.A., Mjelle, R., Hagen, L., Sousa, M.M.L., Krokan, H.E., and Kavli, B. (2019). Uracil-DNA glycosylase UNG1 isoform variant supports class switch recombination and repairs nuclear genomic uracil. Nucleic Acids Res. 47, 4569–4585. https://doi. org/10.1093/nar/gkz145.
- Paone, A., Marani, M., Fiascarelli, A., Rinaldo, S., Giardina, G., Contestabile, R., Paiardini, A., and Cutruzzolà, F. (2014). SHMT1 knockdown induces apoptosis in lung cancer cells by causing uracil misincorporation. Cell Death Dis. 5, e1525. https://doi.org/10.1038/cddis.2014.482.
- Matos, D.A., Zhang, J.M., Ouyang, J., Nguyen, H.D., Genois, M.M., and Zou, L. (2020). ATR Protects the Genome against R Loops through a MUS81-Triggered Feedback Loop. Mol. Cell 77, 514–527.e4. https://doi. org/10.1016/j.molcel.2019.10.010.





STAR***METHODS**

KEY RESOURCES TABLE

REAGENT or RESOURCE	SOURCE	IDENTIFIER
Antibodies		
8-Hydroxy-2'-deoxyguanosine	Abcam	ab48508; RRID:AB_867461
UNG	Novus	NBP1-49985; RRID:AB_10012175
HA	BioLegend	901501
MCM2	Bethyl	A300-191A; RRID:AB_162709
SMUG1	Abcam	ab192240
MBD4	Abcam	ab224809
TDG	Abcam	ab154192
dUTPase	Abcam	ab137097
PrimPol	Home made; Mourón et al.39	N/A
RPA32 pS33	Bethyl Laboratories	A300-246A; RRID: AB_2180847
CHK1 pS317	Cell Signaling Technology	2344T; RRID: AB_331488
53BP1	Millipore	MAB3802; RRID: AB_2206767
Cyclin A	Santa Cruz	sc-751; RRID: AB_631329
γH2AX	BD Biosciences	560443; RRID: AB_1645592
MUS81	Abcam	ab14387
Anti-BrdU rat (for DNA fiber)	Abcam	ab6326; RRID: AB_305426
Anti-BrdU mouse (for DNA fiber)	BD Biosciences	347580; RRID: AB_400326
Goat Anti-Rat Alexa Fluor 594 (For DNA fiber)	Invitrogen	A-11007; RRID: AB_10561522
Goat Anti-Mouse Alexa Fluor 488 (For IF and DNA fiber)	Invitrogen	A-11001; RRID: AB_2534069
Goat Anti-Rabbit Alexa Fluor 488 (For IF)	Jackson ImmunoResearch	111-545-144; RRID: AB_2338052
Goat Anti-Mouse Alexa Fluor 594 (For IF)	Jackson ImmunoResearch	115-585-003; RRID: AB_2338871
Anti-HRP rabbit (for WB)	Jackson ImmunoResearch	111-035-003; RRID: AB_2313567
Anti-HRP mouse (for WB)	Jackson ImmunoResearch	115-035-003; RRID: AB_10015289
Anti-HRP rat (for WB)	Jackson ImmunoResearch	112-035-003; RRID: AB_2338128
RPA32	Thermo Fisher Scientific	MA1-26418, RRID: AB_795362
Pol ε catalytic subunit A	Novus	NBP2-55332
Chemicals, peptides, and recombinant proteins		
PureLink™ RNase A	Thermo Fisher Scientific	12091-021
OGG1i (TH5487)	Selleckchem	S8913
Lipofectamine RNAiMAX	Thermo Fisher Scientific	13778-150
Lipofectamine3000	Thermo Fisher Scientific	L3000015
ATRi (VE-821)	Selleckchem	S8007
ATRi - Ceralasertib (AZD6738)	Selleckchem	S7693
Uracil-DNA Glycosylase	Roche	11444646001
CometAssay LMAgarose	Bio-Techne	4250-050-02
Doxycycline hyclate	Sigma-Aldrich	D9891
CIdU	Sigma-Aldrich	C6891
dU	Sigma-Aldrich	17125
Thymidine	Sigma-Aldrich	T1895
Hydroxyurea	Sigma-Aldrich	H8627
S1 Nuclease	Thermo Fisher Scientific	18001-016
Pemetrexed	Selleckchem	S1135
TAS-114	MedChem Express	HY-124062

(Continued on next page)

Molecular Cell

Article



Continued		
REAGENT or RESOURCE	SOURCE	IDENTIFIER
BioTracker NTP-Transporter Molecule	Sigma-Aldrich	SCT064
Cy3-dUTP	ApexBio	B820
dUTP PCR Grade, sodium salt	Sigma-Aldrich	SKU 11934554001
dTTP PCR Grade, sodium salt	Sigma-Aldrich	SKU 11934546001
Leibovitz's L-15 Medium	Gibco	11415064
302	MedChem Express	HY-101462
ΓLS _{pp}	N/A	Dash et al. ⁶³ ,Stanzione et al. ⁶⁴
Critical commercial assays		
CellTiter-Glo® Luminescent	Promega	G7570
DENTR™/D-TOPO Cloning Kit	Thermo Fisher Scientific	45-0218
Gateway LR Clonase™ II Enzyme mix	Thermo Fisher Scientific	11791-020
Duolink® In Situ Red Starter Kit Mouse/Rabbit	Sigma-Aldrich	DUO92101
DNA Damage Assay Kit (AP sites, Colorimetric)	Abcam	ab211154
NucleoSpin RNA kit for RNA purification	Macherey-Nagel	740955
Deposited data		
Unprocessed western blots, gels, and images	This paper	[https://doi.org/10.17632/f5nd33vw8x.1]
Experimental models: Cell lines		
J20S	ATCC	HTB-96
J2OS UNG2 KO Clone 1	Generated in this study	N/A
J2OS UNG2 KO Clone 2	Generated in this study	N/A
J2OS+pINDUCER20	Generated in this study	N/A
J2OS+WT UNG2-HA (Dox inducible)	Generated in this study	N/A
HEK293T	ATCC	CRL-11268
H1299	MGH CMT	N/A
H1975	MGH CMT	N/A
H1838	MGH CMT	N/A
A 549	MGH CMT	N/A
Calu-1	MGH CMT	N/A
RPE-1	ATCC	CRL-4000
MGH 134.1	Hata Lab	N/A
MGH 707.1	Hata Lab	N/A
MGH 143-3B	Hata Lab	N/A
Oligonucleotides		
Primers for cloning	This study	See STAR Methods below
siRNA sequences	This study	See STAR Methods below
Primers for RT-qPCR	This study	See STAR Methods below
Recombinant DNA		300 0.7
UNG (NM_080911) Human Tagged ORF Clone	Origene	RC222868
bINDUCER20	Meerbrey et al. ⁶⁵	Addgene 44012
DINDUCER20+WT UNG2-HA	Generated in this study	N/A
Software and algorithms	deficiated in this study	. 4// \
GraphPad Prism 6	GraphPad Software, Inc	https://www.graphpad.com/
NIS Elements Viewer	Nikon	https://www.microscope.healthcare.
AIO FIGHICINO AIGMOI	ININOIT	nikon.com/products/software/ nis-elements/viewer
FIJI	N/A	https://imagej.net/software/fiji/
	1 1// 1	Titipo.//iiTiagoj.Tio/ software/ fiji/





RESOURCE AVAILABILITY

Lead contact

Please direct any requests for further information or reagents to the lead contact, Professor Lee Zou (lee.zou@duke.edu), Department of Pharmacology and Cancer Biology, Duke University School of Medicine, Durham, NC 27710.

Materials availability

All materials generated in this study are available through lead contact upon request.

Data and code availability

- Uncropped blots, gels, and microscopy images are available through Mendeley [https://doi.org/10.17632/f5nd33vw8x.1].
- This paper does not report any original code.
- Any additional information required to reanalyze the data reported in this paper is available from the lead contact upon request.

EXPERIMENTAL MODEL AND STUDY PARTICIPANT DETAILS

Cell culture

The human embryonic kidney cell line HEK293T, the hTERT-immortalized human retinal pigment epithelial cell line RPE-1, the human osteosarcoma cell line U2OS and Its derivative UNG2 KO cell lines were maintained in Dulbecco's modified Eagle's medium (DMEM) supplemented with L-glutamine, 10% Fetal Bovine Serum (FBS), and 1% penicillin/streptomycin (PS). Human lung cancer cell lines H1299, H1838, and H1975 were maintained in RPMI 1640 medium supplemented with 10% FBS and 1% PS. The human lung cancer cell line A549 was maintained in F-12K medium supplemented with 10% FBS and 1% PS. The human lung cancer cell line Calu-1 was maintained in McCoy's 5A medium supplemented with 10% FBS and 1% PS. U2OS KO cell lines expressing pINDUCER20 empty vector/UNG2-HA were generated by infecting the cells with lentivirus expressing UNG2-HA under a doxycycline-inducible promoter (pINDUCER20) and selected with G418 (400 μ g/mL). Patient-derived cell lines MGH 707.1, ⁶⁶ MGH 134.1 ^{67,68} and MGH143-3B ⁶⁹ were established at Massachusetts General Hospital from non-small cell lung cancer core biopsy or pleural effusion samples. All patients signed informed consent to participate in a Dana Farber/Harvard Cancer Center Institutional Review Board-approved protocol giving permission for research to be performed on their samples. Cell lines were sequenced to confirm the presence of oncogenic driver mutations.

METHOD DETAILS

Cloning

The human *UNG* ORF clone was purchased from Origene (Catalog#: RC222868). From this plasmid, *UNG2* was amplified and cloned into the pENTR-TOPO Gateway vector. For lentiviral expression, pENTR-TOPO-UNG2 was inserted into pINDUCER20 carrying an HA tag at the C terminus. The endogenous stop codon of *UNG2* was removed to allow in-frame expression of the C-terminal HA tag. The primers used are as follows:

Primer name	Description	Sequence (5'-3')
SS_5	hsUNG2_Topo cloning_Forward	CACCATGATCGGCCAGAAGACGCTCTACTCC
SS_7	hsUNG2_Reverse_without stop codon	CAGCTCCTTCCAGTCAATGGGCTT

CRISPR-Cas9 KO cell lines

UNG2 was knocked out in U2OS cells using sgRNAs previously described. 70

Forward: caccgCGTCTTCTGGCCGATCATCC

Reverse: aaacGGATGATCGGCCAGAAGACGc

The sgRNAs targeting exon 1A of human UNG2 were cloned into PX458 vector. U2OS cells were transfected with gRNA-expressing plasmids. After 3 days, GFP-positive cells were sorted into 96-well plates as single cells by FACS and grown for 3 weeks before the cells were transferred to 24-well plates. Loss of UNG2 protein was verified by western blot using UNG antibody and 2 clones were selected for further studies.

Plasmid transfection

For viral production and plasmid transfection, HEK293T and U2OS cells were transfected using Lipofectamine 3000 (Thermo Fisher Scientific) following manufacturer's instructions.

Molecular Cell

Article



RNA interference

Reverse siRNA transfections were done using 5-10 nM Silencer Select pre-designed siRNAs (Thermo Fisher Scientific) with Lipofect-amine RNAiMAX (Thermo Fisher Scientific) for 48 hours. We used siDESIGN Center (Horizon Discovery) to design siRNA (siUNG#4) targeting the 3'UTR region of UNG mRNA (Thermo Fisher Scientific).

siRNAs used in this study	Sequence (5'-3') or ID
Control	Thermo Scientific: 4390843
UNG#1	Thermo Scientific: s14679
UNG#2	Thermo Scientific: s14678
UNG#4 (3' UTR)	UGGAAUAAGCAGUGGAAUUtt
SMUG1	Thermo Scientific: s24135
MBD4	Thermo Scientific: s17077
TDG	Thermo Scientific: s13950
MUS81	CAGCCCUGGUGGAUCGAUAtt
DUT	Thermo Scientific: s4390
PrimPol	Thermo Scientific: s47416
OGG1	UCCAAGGUGUGCGACUGCUtt

Quantitative real-time PCR

Total RNA was isolated using NucleoSpin RNA kit for RNA purification (Macherey-Nagel; 740955). Reverse transcription was carried out with 1 μ g of total RNA using random hexamer primers and the SuperScript IV reverse transcriptase kit (Thermo Fisher Scientific). Quantitative PCR was performed using Kapa SYBR Green on a Lightcycler 480 (Roche). mRNA expression relative to *GAPDH* mRNA levels was calculated using the delta-delta threshold cycle ($\Delta\Delta$ CT) method. The primers used are as follows:

Primer name	Description	Sequence (5'-3')
UNG1_F	Forward primer for qPCR-UNG1	ATGGGCGTCTTCTGCCTTG
UNG1_R	Reverse primer for qPCR-UNG1	CTCTGGATCCGGTCCAACTG
UNG2_F	Forward primer for qPCR-UNG2	GCCAGAAGACGCTCTACTCC
UNG2_R	Reverse primer for qPCR-UNG2	GCATCTCCGCTTTCCTCA
GAPDH_F	Forward primer for qPCR-GAPDH	CGGAGTCAACGGATTTGGTCGTA
GAPDH_R	Reverse primer for qPCR-GAPDH	AGCCTTCTCCATGGTGGTGAAGAC
OGG1_F	Forward primer for qPCR-OGG1	ACTAGCGGATCAAGTATGGACA
OGG1_R	Reverse primer for qPCR-OGG1	CAGGGTAACATCTAGCTGGAAG

Measurement of AP sites

AP-sites were tested in U2OS cells 48 h after transfection with control and UNG siRNA by a DNA damage assay kit (ab211154, Abcam) according to the manufacturer's instructions.

U-comet assay

The comet assay was performed as previously described. ⁷¹ U2OS, H1299, H1838, MGH 134.1, MGH 707.1 and MGH 143-3B cells were treated with drugs as indicated, harvested, washed with PBS, and then mixed with low-melt agarose (Sigma Aldrich) at 37 °C and embedded on 1% agarose-coated Superfrost slides (Bio-Techne R&D Systems). Subsequent steps were carried out away from light. Slides were submerged in lysis buffer (2.5 M NaCl, 100 mM EDTA, 10 mM Tris, 10% DMSO, 1% Triton X-100, 8 mg/ml NaOH to pH 10) for 2 hours at 4°C, washed 3 times with enzyme buffer (20 mM Tris-HCl, 1 mM DTT, 1 mM EDTA pH 8), then treated with uracil-DNA glycosylase (Roche, UNG 0.01 unit/slide diluted in enzyme buffer) or enzyme buffer only for 1 hour at 37°C. Slides were denatured in electrophoresis buffer (1 mM EDTA, 300 mM NaOH) for 30 min at room temperature (RT), then subjected to electrophoresis at 22 V and 300 mA for 60 min at 4°C, followed by incubation in neutralization buffer (400 mM Tris, HCl to pH 7.5) for 45 min at RT. For image acquisition, slides were stained with SYBR® Gold Nucleic Acid Gel Stain (ThermoFisher) and visualized at 488 nm and 10x magnification using a Nikon 90i microscope. Comet tail moment for 100-200 cells per condition was measured using ImageJ OpenComet plugin.



Molecular Cell Article

High-performance liquid chromatography-mass spectrometry measurement of genomic deoxyuridine

Genomic DNA was purified from 10-15 million cells using Zymo Quick DNA midiprep Kit (Product #D4075) per manufacturer's recommendations. DNA was eluted in DNase/RNase-free water and dried over gaseous N₂. Total DNA yields were measured using Invitrogen Qubit dsDNA BR assay (Product #Q32851) and recorded for subsequent normalization of mass spectrometry data. Typical yields ranged from 10-20 micrograms of DNA. Deoxyuridine content was measured by treatment of DNA with Uracil DNA Glycosylase (UDG), which generates free uracil nucleobase. DNA was resuspended in UDG reaction buffer (10 mM Tris HCl, pH 8.0@25°C, 1 mM EDTA, 1 mM DTT) containing 50 fmol of stable, isotopically labeled 1,3-¹⁵N₂ Uracil (Cambridge Isotope Laboratories, Catalog number NLM-637-0; Lot Number PR32662B). *E. Coli* UDG (New England Biolabs Inc., Catalog number M0280L, Lot number 10151474) was dialyzed twice in 1000 sample volumes of UDG reaction buffer at 4°C for 12 hours to remove glycerol from enzyme concentration. 10U of UDG enzyme was added to 100 uL of genomic DNA resuspended in UDG reaction buffer and incubated at 37°C for 2 hours. Samples were then spin-filtered with Amicon Ultra 0.5 mL Centrifugal filters with 3 kilodalton molecular weight cutoff (Catalog number UFC500396). Eluate was dried over gaseous N2 and stored at -80°C prior to analysis by High Performance Liquid Chromatography-Mass Spectrometry (LC-MS).

On the day of LC-MS analysis, samples were resuspended in 20 µl high-performance liquid chromatography-grade Water (Sigma-Aldrich, Catalog number 270733-4L). Metabolites were measured using a Dionex UltiMate 3000 ultrahigh-performance liquid chromatography system connected to a Q Exactive benchtop Orbitrap mass spectrometer, equipped with an Ion Max source and a HESI II probe (Thermo Fisher Scientific). Samples were separated by chromatography by injecting 2 µl of sample on a SeQuant ZIC-pHILIC Polymeric column (2.1 × 150 mm 5 µM, EMD Millipore). Flow rate was set to 150 µl min⁻¹, temperatures were set to 25 °C for column compartment and 4 °C for autosampler sample tray. Mobile Phase A consisted of 20 mM ammonium carbonate, 0.1% ammonium hydroxide. Mobile Phase B was 100% acetonitrile. The mobile phase gradient (%B) was set in the following protocol: 0–20 min, linear gradient from 80% to 20% B; 20–20.5 min, linear gradient from 20% to 80% B; 20.5–28 min, hold at 80% B. Mobile phase was introduced into the ionization source set to the following parameters: sheath gas, 40; auxiliary gas, 15; sweep gas, 1; spray voltage, –3.1 kV; capillary temperature, 275 °C; S-lens RF level, 40; probe temperature, 350 °C. Metabolites were monitored with a full-scan and additional narrow range scan (110.5–113.5 m/z) in negative mode only. The resolution was set at 70,000, the AGC target at 1,000,000 and the maximum injection time at 20 ms. Relative quantitation of metabolites was performed with XCalibur QuanBrowser 2.2 (Thermo Fisher Scientific) using a 5 ppm mass tolerance and referencing an retention time for uracil from an inhouse library of chemical standards. Total ion counts were normalized to the internal 1,3-¹⁵N₂-labelled uracil standard and nanograms of input genomic DNA per sample.

DNA fiber analysis

Exponentially growing U2OS, H1299 or H1838 cells were first pulse labeled with 100 μ M CldU, washed twice with equilibrated complete media and then labeled with 250 μ M IdU under the conditions specified in the figure legends. Collected cells were resuspended in cold PBS (1x10⁶ cell per milliliter), and 3 μ L of cell suspension was mixed with spreading buffer (8 μ L) (0.5% SDS, 200 mM Tris-HCl pH 7.4, 50 mM EDTA) and let spread by gravity on a tilted glass slide. DNA fibers were fixed in methanol:acetic acid (3:1) for 10 min, denatured in 2.5 N HCl for 60 min, and blocked in 3% BSA/0.05% Tween-20 for 30 min at 37°C. CldU and IdU detection were done using rat anti-BrdU (1:100; Abcam) and mouse anti-BrdU (1:50; BD Biosciences) for 1 hour at 37°C followed by Alexa 488 anti-mouse (1:100; Jackson ImmunoResearch) and Cy3 anti-rat (1:100; Jackson ImmunoResearch) for 30 minutes at 37°C. Slides were mounted with Prolong Gold and dried overnight. Fibers were imaged with a 60X objective on a Nikon 90i microscope. FIJI software was used to quantify immunofluorescence intensities and measure IdU tract length. One-way ANOVA with Tukey's multiple comparisons test was used to measure the significance.

S1 nuclease experiments were essentially performed as described previously. ⁴⁰ After IdU labeling, cells were permeabilized with CSK100 buffer (100 mM NaCl, 10 mM MOPS pH7, 3 mM MgCl2, 300 mM sucrose, 0.5% Triton X-100) for 10 minutes at RT and then washed with 1x PBS carefully. The cells were washed once with S1 nuclease buffer pH4.6 (30 mM NaAc, 10 mM ZnAc, 5% glycerol, 50 mM NaCl) and subsequently incubated with S1 buffer containing S1 nuclease (20 U/ mL) for 30 minutes at 37°C. The cells were washed once with 1x PBS containing 0.1% BSA to help precipitate nuclei, then collected and processed for staining as described above.

Uracil excision activity assay

U2OS cells were transfected with control or UNG siRNA and lysed in native lysis buffer (25 mM HEPES pH 7.9, 10% glycerol, 150 mM NaCl, 0.5% Triton X-100, 1 mM EDTA, 1 mM MgCl2, 0.2 μ g/ml RNase A and protease inhibitors) after 48 h. Cell lysates were sonicated, incubated for 30 min at 4°C, and then centrifuged for 10 min at 13,000 RPM at 4°C. Protein concentration was determined by BCA Assay (Thermo Fisher Scientific) and extracts were normalized. 20 uL aliquots were prepared and flash frozen in liquid nitrogen and stored in -80°C. A fresh vial of extract was used for each experiment.

For the activity assay, normalized amounts of cell extracts were incubated with $0.4~\mu M$ DNA hairpin substrate for 1 h at $37^{\circ}C$ in reaction buffer (50 mM Tris pH 7.5, 0.1~mg/ml RNase A, and 5 mM EDTA). DNA oligonucleotide probe was synthesized by ThermoFisher Scientific having the following sequence: 5/FAM-GCAAGCCTTUGGCTTGCTGA. For the positive control, DNA substrate was incubated with 1 unit of purified Uracil-DNA glycosylase (New England BioLabs) instead of cell extracts in the same reaction buffer. After 1 h, 100~mM NaOH was added to the reaction and further incubated at $95^{\circ}C$ for 30 min to cleave AP-sites.

Molecular Cell Article



Gel loading buffer (0.5% Orange G in Formamide) at 1:1 concentration was then added to the reaction and further incubated at 95°C for 10 min, spun down and kept on ice for 5 min. A 20% denaturing polyacrylamide gel (8 M urea, 1× TAE buffer) was pre-run in 1X TAE buffer for 10 min and 10 uL samples were loaded. DNA cleavage was monitored by running the gel for 90 min at 150 V. The gel was analysed on a Chemidoc imaging system (BioRad) with ImageLab v6.0.1 software. Quantification was performed using Fiji.

Import of dNTPs into live cells

U2OS cells were treated with 2 μ M Bio-tracker (BT) and indicated concentrations of Cy3-dUTP, dUTP or dTTP for 24 h in Leibovitz's L-15 Medium supplemented with 10% FBS and 1% PS. For cell survival assays, after 24 h treatment with BT and Cy3-dUTP, the cells were seeded in 96-well plates in fresh DMEM supplemented with L-glutamine, 10% FBS, and 1% PS and indicated concentrations of ATRi and cultured for 5-7 days.

Immunofluorescence

To monitor DNA synthesis, U2OS cells were pulse-labeled with 10 μ M EdU for 30 minutes and then treated as described in the figure legends. Cells were pre-extracted with 1x PBS containing 0.2% Triton X-100 for 2 minutes prior to fixation with 3% paraformaldehyde/2% sucrose for 10 min at RT. Following two washes with 3% BSA in 1x PBS, coverslips were incubated with 2 mM CuSO4, 10 mM sodium ascorbate, and 1 μ M picolyl-azide AF647 in 1x TBS for 30 minutes at RT, followed by two washes with 3% BSA in 1x PBS. Coverslips were then incubated with the IF blocking buffer (1% BSA+0.5% T-X100 in 1x PBS) for 60 min at RT. Primary antibodies diluted in blocking buffer were added to the cells, and incubation continued for 2 hours at RT. After two washes with PBST (1x PBS with 0.5% T-X100), cells were incubated in the dark with secondary antibodies, diluted to 1:250 in blocking buffer, for 1 hour at RT. Finally, after two washes with PBST, cells were stained with DAPI for 5 minutes and mounted on slides with Prolong Gold. Images were captured with a Nikon 90i microscope and quantified using FIJI.

For 8-oxoG immunostaining, coverslips were fixed in 3% paraformaldehyde/2% sucrose for 20 min at RT, followed by permeabilization in 1x PBS containing 0.5% Triton X-100 for 5 minutes. Next, coverslips were treated with RNAse buffer (1 mM EDTA, 10 mM Tris-HCl (pH 7.5), 0.4 mM NaCl, and 100 μ g/mL RNAse (Invitrogen) for 1 hour at 37°C, followed by denaturation in 2.5 N HCl for 30 min at RT. After two washes and 10 min incubation in neutralization buffer (50 mM Tris-HCl pH 8.8) at RT, coverslips were blocked with 4% BSA+0.1% T-X100 in PBS for 1 hour at RT. Primary antibodies diluted in blocking buffer were added to the cells, and incubation continued overnight at 4°C. After two washes with PBST (1x PBS with 0.5% T-X100), cells were incubated in the dark with secondary antibodies, diluted to 1:250 in blocking buffer, for 1 hour at RT. Finally, after two washes with PBST, cells were stained with DAPI for 5 minutes and mounted on slides with Prolong Gold. Images were captured with a Nikon 90i microscope and quantified using FIJI.

Proximity ligation assay

PLA was performed as described previously. Pirefly, cells were treated with CSK extraction buffer (0.2% Triton X-100, 20 mM HEPES-KOH pH 7.9, 100 mM NaCl, 3 mM MgCl2, 300 mM sucrose, 1 mM EGTA), fixed with PFA and methanol, and then permeabilized with 1x PBS containing 0.5% Triton-x100. The cells were treated with RNaseA (10 ug/ml) for 1 hour at 37 °C and then washed and blocked with 3% BSA in PBST buffer for 1 hour. The cells were incubated with the primary antibodies diluted at 1:500 at 4°C overnight. After three washes with 1x PBST, the cells were incubated with anti-mouse minus and anti-rabbit plus PLA probes (PLA kit from Sigma) at 37°C for 1 hour. The cells were washed with PLA buffer A and incubated with ligation buffer containing ligase (PLA kit) for 30 minutes at 37°C, then washed and incubated with amplification buffer with polymerase (PLA kit) at 37°C for 1 hour. The cells were washed twice with PLA buffer B (PLA kit) and then three times with PBST buffer containing DAPI. Images were captured with a Nikon 90i microscope.

Immunoblots

Cells were harvested and lysed in RIPA buffer supplemented with 1x protease inhibitors. Protein concentrations were normalized using Bradford assay and mixed 1:1 with 2× SDS PAGE loading buffer (100 mM Tris at pH 6.8, 12% glycerol, 3.5% SDS, 0.2 M DTT). Samples were boiled for 10 minutes, loaded on Bolt Bis-Tris Plus 4%–12% gels, and run at 100 V for 90 min. Proteins were transferred onto PVDF membranes using a CBS Scientific electrophoretic blotting liquid transfer system (EBX-700) for 1 hour at 300 mA. Membranes were then blocked in Tris-buffered saline with 0.05% Tween-20 (TBS-T) and 3% BSA for 60 min at RT. Membranes were then immunoblotted with primary antibodies, diluted in blocking buffer, overnight at 4°C with mild shaking. The PrimPol antibody was kindly provided by the Méndez laboratory. Membranes were washed twice for 5 min with TBST and incubated for 2-3 hours at 4°C with secondary antibodies conjugated to horseradish peroxidase. Membranes were washed twice for 5 minutes with TBST and an enhanced chemiluminescence (ECL Bio-Rad 1705061) solution was applied. Signals were detected using a Chemidoc imaging system (Bio-Rad) with ImageLab v6.0.1. software.

Chromatin fractionation

Cells were harvested and washed with PBS. Cytosolic proteins were removed by incubation of cells in hypotonic buffer (10 mM HEPES-KOH pH 7.5, 5 mM KCl, 1.5 mM MgCl2, 1 mM DTT and 0.5% NP-40) for 15 minutes on ice and centrifuged at 13000 rpm for 5 minutes. The nucleus-enriched pellets were resuspended in fraction buffer (10 mM HEPES-KOH pH 7.5, 5 mM KCl, 1.5 mM MgCl2, 1 mM DTT and 0.5% NP-40 and 0.5 M NaCl), incubated on ice for 10 minutes and centrifuged at 13000 rpm for 5 minutes.





The supernatants containing soluble nuclear proteins was discarded and the chromatin-enriched pellets were washed once with fraction buffer. The final pellets enriched for stably chromatin-bound proteins were incubated in 2x Laemmle sample buffer for 10 minutes at 90°C and used for western blotting.

Primer extension assay

The following DNA oligomers were purchased from Integrated DNA Technologies, Inc. and purified using denaturing urea polyacrylamide gel electrophoresis (PAGE) as described previously.³⁴

Oligomer	Sequence (5'-3')
1U template	GGAGACAAGCTTGA <u>U</u> TGCCTCGAGGTCGACTCTAGCGGCTCCCC
1T template	GGAGACAAGCTTGA <u>T</u> TGCCTCGAGGTCGACTCTAGCGGCTCCCC
2U template	GGAGACAAGCTTG <u>UU</u> TGCCTCGAGGTCGACTCTAGCGGCTCCCC
2T template	GGAGACAAGCTTG <u>TT</u> TGCCTCGAGGTCGACTCTAGCGGCTCCCC
Primer	GGGGAGCCGCTAGAGTCGACCTC

The DNA primer 23-mer was radiolabeled by incubating with $[\gamma^{-32}P]$ ATP (Revvity) and T4 polynucleotide kinase (NEB) at 37°C for 3 hours. After the labeling reaction, the reaction was stopped by heating the mixture at 95°C for 5 minutes. After T4 kinase inactivation, any unreacted $[\gamma^{-32}P]$ ATP in the mixture was removed by using a Bio-Spin 6 column (Bio-Rad). The 5′-radiolabeled 23-mer was mixed with each of the unlabeled DNA templates in the molar ratio of 1:1.2. For the primer and template annealing, the mixture was first heated to 95°C for 5 minutes and then cooled slowly to RT overnight.

The exonuclease-deficient triple mutant (D275A/E277A/D368A) form of the truncated human DNA polymerase ε catalytic subunit (hPol ε exo $^-$) was overexpressed and purified as described previously. The assays were performed by adding a solution of dATP, dGTP, dCTP, and dTTP (100 μ M each; Invitrogen) to the preincubated solution of hPol ε exo $^-$ and 5'-labeled 100 nM 23-mer/44-mer duplex in 1x reaction buffer (50 mM HEPES (pH 7.5), 5 mM MgCl2, 50 mM NaCl, 0.1 mM EDTA, 5 mM DTT, 10% glycerol, and 0.1 mg/ml of BSA) for 0, 8, 15, and 30 seconds at RT before the reactions were quenched with 0.37 M EDTA. All concentrations reported are final after mixing. The reaction products were analyzed by using denaturing PAGE (17% acrylamide, 8M Urea) and imaged by Typhoon TRIO (GE Healthcare).

Cell viability assay

Cell viability assays were performed in 96-well format and cells were treated as described in the figure legends. To determine the number of viable cells, CellTiter-Glo was used according to manufacturer's instructions.

In vivo drug response

2 x 10⁶ H1299 non-small cell lung carcinoma cells were injected into the right flank of female NOD scid gamma (NSG) mice (Jackson Laboratory) in equal proportions with Matrigel Basement Membrane Matrix (Corning, CLS354234). Tumors were allowed to reach 100±5 mm³ prior to beginning treatment. Four mice were treated per cohort. Mice were administered either intraperitoneal injections of Pemetrexed (Selleckchem, S5971) in 0.9% NaCl (75 mg/kg), AZD6738 (Selleckchem, S7693) in 5% DMSO and 40% propylene glycol (50 mg/kg), or both. Control mice were administered equal amounts of DMSO via the same route. Mice were treated every other day for a total of 15 treatments. Tumors were measured externally using calipers and tumor volume was calculated using the following formula: (length x width²)/2. Mice were weighed once a week to monitor changes in weight.

QUANTIFICATION AND STATISTICAL ANALYSIS

All statistical analyses were performed using Prism (GraphPad software). The number of replicates, statistical parameters, and tests are reported in the figure legends. Unless indicated otherwise, one-way ANOVA with Tukey's multiple comparisons test was used to measure the significance throughout. p value significance was defined as follows: (ns) non-significant; (*) $P \le 0.05$; (**) $P \le 0.01$; (***) $P \le 0.001$.